STABILITY AND ELECTRONIC STRUCTURE OF MAGNESIUM HYDRIDE AND
MAGNESIUM DEUTERIDE UNDER HIGH PRESSURE

Mr. Chayaphon Boonchot

A Thesis Submitted in Partial Fulfillment of the Requirements

for the Degree of Master of Science in Physics

Department of Physics

FACULTY OF SCIENCE

Chulalongkorn University

Academic Year 2021

เสถียรภาพและอิเล็กทรอนิกของโครงสร้างแมกนีเซียมไฮไดรด์และแมกนีเซียมดิวเทอเรียมภายใต้แรงดันสูง

นายชยพล บุญโชติ

Thesis Title	STABILITY AND ELECTRONIC STRUCTURE OF MAGNESIUM HYDRIDE AND MAGNESIUM DEUTERIDE UNDER HIGH PRESSURE
By	Mr. Chayaphon Boonchot
Field of Study	Physics
Thesis Advisor	Associate Professor Dr. UDOMSILP PINSOOK
Thesis Co Advisor	Dr. Prutthipong Tsuppayakorn-aek

Accepted by the FACULTY OF SCIENCE, Chulalongkorn University in Partial Fulfillment of the Requirement for the Master of Science

　　　　　　　　　　　　　　　　　　　　　　　 Dean of the FACULTY OF SCIENCE

(Professor Dr. POLKIT SANGVANICH)

THESIS COMMITTEE

　　　　　　　　　　　　　　　　　　　　　　 Chairman

(Associate Professor Dr. NAKORN PHAISANGITTISAKUL)

　　　　　　　　　　　　　　　　　　　　　　 Thesis Advisor

(Associate Professor Dr. UDOMSILP PINSOOK)

　　　　　　　　　　　　　　　　　　　　　　 Thesis Co-Advisor

(Dr. Prutthipong Tsuppayakorn-aek)

　　　　　　　　　　　　　　　　　　　　　　 Examiner

(Assistant Professor Dr. RANGSIMA CHANPHANA)

　　　　　　　　　　　　　　　　　　　　　　 External Examiner

(Dr. Teeraphat Watcharatharapong)

ชยพล บุญโชติ : เสถียรภาพและอิเล็กทรอนิกของโครงสร้างแมกนีเซียมไฮไดรด์และแมกนีเซียมดิวเทอเรียมภายใต้แรงดันสูง. (STABILITY AND ELECTRONIC STRUCTURE OF MAGNESIUM HYDRIDE AND MAGNESIUM DEUTERIDE UNDER HIGH PRESSURE) อ.ที่ปรึกษาหลัก : รศ. ดร.อุดมศิลป์ ปิ่นสุข, อ.ที่ปรึกษาร่วม : ดร.พฤทธิพงษ์ ทรัพยากรเอก

โลหะโพลีไฮไดรด์ได้รับความสนใจเนื่องจากความสามารถในเปลี่ยนเป็นโลหะภายใต้ความดันสูงได้ ในขณะที่บางชนิดอาจเริ่มเปลี่ยนเฟสเพื่อกลายเป็นตัวนำยิ่งยวด มีการค้นพบว่าโลหะโพลีไฮไดรด์กลายเป็นตัวนำยิ่งยวดที่มีอุณหภูมิวิกฤต (T_c) สูงภายใต้แรงดันในงานครั้งนี้เราคำนวณโครงสร้างของ
MgH_2(FCC), MgH_2 (HCP) และ MgH_3 ภายใต้แรงดันตั้งแต่ 0-300 GPa เพื่อศึกษารูปแบบของเอนทัลปีและคุณสมบัติทางอิเล็กทรอนิกส์ของโครงสร้างภายใต้แรงดันสูง เรายังแทนที่อะตอมของไฮโดรเจนด้วยดิวเทอเรียม (D) โดยพลังงานทั้งหมดจะถูกคำนวณและนำไปใช้ในการศึกษาโครงสร้างทางอิเล็กทรอนิกส์ ความหนาแน่นของสถานะ และการกระจายตัวของโฟนอน เป็นหลักเราพบว่ากราฟ Convex hulls ของ MgH_2(HCP)นั้นไม่เสถียรในทุกความดันส่วน MgH_3 นั้นจะเสถียรที่ 100-300 GPa และ MgH_2(FCC)นั้นเสถียรอยู่ที่ 0-200 GPa ซึ่งเป็นความเสถียรเชิงเทอร์โมไดนามิกส์ดังนั้นเราจึงไม่คำนวณโฟนอนและสมบัติอื่นๆของโครงสร้างMgH_2 (HCP) ผลการคำนวณโฟนอนของโครงสร้าง MgH_3 ยืนยันความเสถียรของโครงสร้างที่ความดันสูงและเราพบว่าความถี่โฟนอนของ MgD_3 ให้ค่าที่ต่ำกว่า MgH_3 อยู่ $1/\sqrt{2}$ เท่าเป็นผลมาจาก isotope effect แต่ผลของการคำนวณโฟนอน MgH_2 (FCC) และ MgD_2 นั้นไม่เสถียรที่ความดัน 0-200 GPa ถึงแม้ว่าจะลองปรับความละเอียดในการคำนวณให้สูงขึ้นแล้วก็ตาม ในส่วนของโครงสร้างอิเล็กทรอนิกส์และความหนาแน่นของสถานะ นั้นพบว่าที่ความดันเดียวกัน ค่าแถบพลังงานและความหนาแน่นของสถานะของ MgH_3 และ MgD_3 นั้นมีค่าที่เหมือนกัน รวมถึงของโครงสร้าง MgH_2 และ MgD_2 เช่นกัน ผลลัพธ์เหล่านี้จะใช้เป็นจุดเริ่มต้นสำหรับการคำนวณอุณหภูมิวิกฤตในอนาคต

สาขาวิชา	ฟิสิกส์	ลายมือชื่อนิสิต
		....
ปี	2564	ลายมือชื่อ อ.ที่ปรึกษาหลัก
การศึกษา		....
		ลายมือชื่อ อ.ที่ปรึกษาร่วม

6270129823 : MAJOR PHYSICS

KEYWORD: The density functional theory (DFT), MgH3, MgH2, MgD2, MgD3, The electrical band structures, The isotope effect, High pressure, Phonon frequencies

Chayaphon Boonchot : STABILITY AND ELECTRONIC STRUCTURE OF MAGNESIUM HYDRIDE AND MAGNESIUM DEUTERIDE UNDER HIGH PRESSURE. Advisor: Assoc. Prof. Dr. UDOMSILP PINSOOK Co-advisor: Dr. Prutthipong Tsuppayakorn-aek

Metal polyhydrides have attracted interest because some of them transform into metals under high pressure, while others initiate a phase transition to become superconductors. It was recently discovered that some superconducting metal polyhydrides have a high critical temperature (T_c) under pressure. We calculate the structures of MgH_2(FCC), MgH_2 (HCP), and MgH_3 under pressures ranging from 0-300 GPa in order to determine the formation enthalpy and electronic properties under high pressure. We also replaced the hydrogen atoms with deuterium (D). The convex hulls of MgH_2(FCC), MgH_2(HCP), and MgH_3(FCC) calculated at pressures from 0 to 300 GPa. At all pressures, MgH_2(HCP) is unstable, whereas MgH_3 is stable between 100 and 300 GPa. MgH_2(FCC) is thermodynamically stable between 0 and 200 GPa. MgH_3 is dynamically stable at high pressure, according to phonon calculations, while MgD_3's phonon frequencies are $1/\sqrt{2}$ times lower than MgH_3's due to the isotope effect. The MgH_2 and MgD_2 results are unstable under pressures ranging from 0 to 200 GPa. The band structures and density of states of MgH_3 and MgD_3 were also described, which appear to be similar, as well as MgH_2 and MgD_2.

Field of Study: Physics   Student's Signature

                                                         ....

Academic   2021   Advisor's Signature

ACKNOWLEDGEMENTS

TABLE OF CONTENTS

LIST OF FIGURES

1. INTRODUCTION

In 1911, Heike Kamerlingh Onnes discovered superconductivity of 4.2 K in mercury [1]. One of the most important activities in condensed matter Physics has been the search for high critical temperature (T_c) superconductors. Copper oxides and iron-based compounds with high superconducting transition temperatures were studied. At ambient pressure, the critical temperature of copper oxides and iron-based superconductors was 133 K [2] and 56 K [3], respectively. The conventional superconductor, magnesium diboride, has a T_c of 39 K [4]. One of the thermodynamic parameters that controls the structure and properties of condensed matter is pressure. High pressure can effectively shorten bonds and change electronic structure, resulting in new phases with unusual structures and properties that are rarely seen at atmospheric pressure. For example, high pressure can make the insulator transform to a metal state [5], increase T_c of superconductors (T_c of copper oxides is raised to 164 K at 31 GPa) [6]. Wigner and Huntington theoretically predicted in 1935 that solid hydrogen would be metalized at high pressure, resulting in metallic hydrogen [7]. As a result, the search for a metallic phase of solid hydrogen has become a hot topic in physics. There are various experimental research projects involving hydrogen at high pressures. However, these studies showed that metallizing hydrogen is extremely difficult. How to reduce the metallic pressure of a hydrogen system is one of the most important topics. In 2004, Aschroft [8] proposed a great idea that hydrogen-rich materials can be metallized at much lower pressures due to 'chemical pre-compression'. High temperature superconductivity can be found after metallization because these materials are dominated by hydrogen elements, which can provide high phonon frequencies and strong electron–phonon coupling (EPC). For room temperature superconductivity, a high Debye temperature and strong electron-phonon coupling are necessary. As a result, they are good candidates for searching for high T_c superconductors within the experimental diamond anvil cell's reach (DAC). Researchers began looking for high-temperature superconductors in hydrogen-rich materials based on this theory. Because

experimental studies of hydrogen-rich materials' metallization and superconductivity under high pressure are difficult, theoretical research has been at the top of the list of this field and made significant contributions. Metal polyhydrides have attracted much interest in condensed matter research since they can turn into superconductors with high critical temperatures when exposed to higher pressures [9]. At 200 GPa, the Mg/Ca substituted hexahydride has shown superconductivity with T_c = 288 K [10]. Magnesium hydrides are the focus of this research (MgH_x). Figure 1 demonstrate different ways to store hydrogen based on volumetric capacity and gravimetric capacity. MgH_2 is interesting for hydrogen storage due to its high gravimetric and volumetric capacities (7.6 wt %and 109 gH_2) [11]. We reported the relative structural stability of MgH_2 (FCC), MgH_2 (HCP), MgH_3 in the pressure range of 0-300 GPa. This work focuses on the structural factors of Magnesium hydride that replaces hydrogen with deuterium. In this work, MgH_2 (FCC), MgH_2 (HCP), MgH_3 structure was chosen as the prototype to find a structure that is stable under high pressure to be used as a base model.
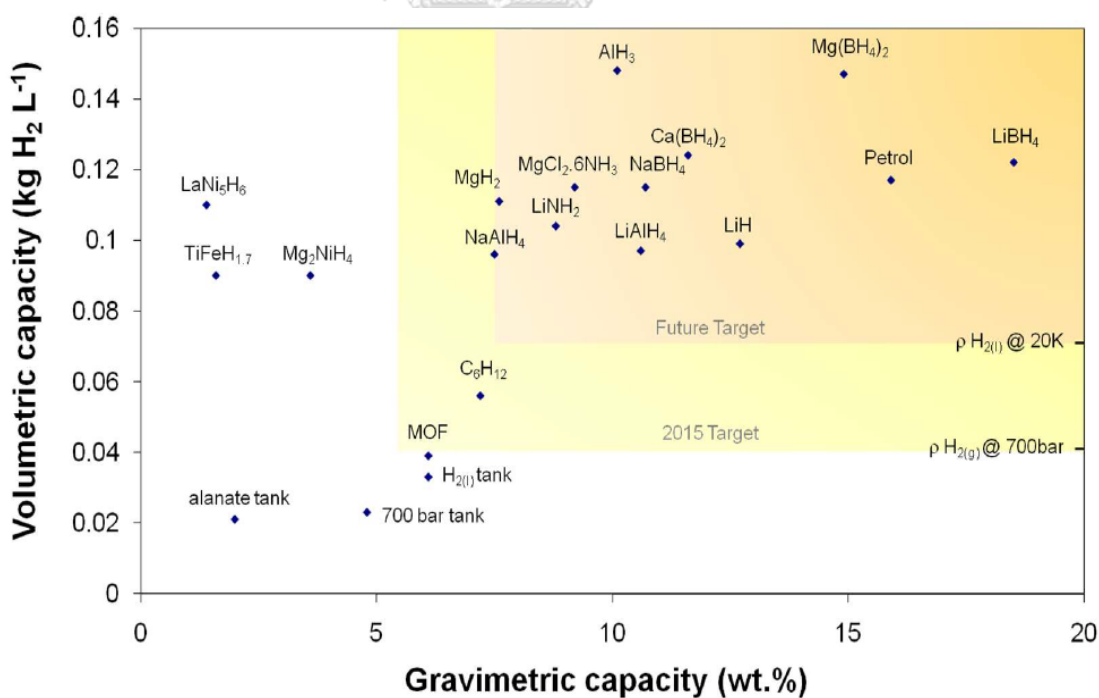
Figure 1 The gravimetric and volumetric capacities of hydrogen for hydrogen fuel [12]

Density Functional Theory (DFT), a method for solving many-body problems, was proposed by Hohenberg and Kohn in 1964 [13]. They demonstrated that the unique ground state properties of a system can be determined by replacing the wave function basis with an electron density by using the exchange-correlation energy which can be solved using the variation method in order to find the exchange-correlation potential, and the exchange-correlation energy can take the form of density. By including the correlation of an electron-electron interaction, or the correlation potential, Kohn proposed the Kohn-Sham equation in 1965 [14]. When the correlation potential is taken into account, the total energy of the many-body system is lower than when the Hartree-Fock equation is solved. As a result, it is thought to produce the most likely relative total energy of the real system. The Kohn-Sham equation is sometimes referred to as "Schrödinger-like," but it is not the same as Schrödinger's equation because it only exists in functional form. W. Kohn was awarded the Nobel Prize in Chemistry in 1998 for this remarkable discovery.

In this work, structural investigation was performed using ab initio methods. All the calculations were performed by using the density functional theory. The self-consistent field method carries out in the Quantum-ESPRESSO code [15]. This research will use the Generalized-Gradient Approximation (GGA) functional of Perdew-Burke-Ernzerhof (PBE) [16] as an exchange-correlation functional.

2. THEORETICAL BACKGROUND

Density Functional Theory

The Density Functional Theory (DFT) is one of the most famous and successful methods for studying ground-state energies and electronic structures in many-body quantum systems. Especially given the fact that they are identical, in concept, several parameter

estimations for exchange-correlation functionals are obligated. A detailed description of the DFT will be discussed in this section.

2.1 The Born-Oppenheimer approximation

The Born-Oppenheimer approximation was the first and most important step in calculating the total energy of a many-body system [17]. The full Hamiltonian can be written as following

$$\hat{H} = -\sum_{i=1}^{N_e} \frac{\hbar}{2m} \nabla^2 - \sum_{i,I} \frac{z_I e^2}{|r_i - R_I|} + \frac{1}{2}\sum_{i \neq j} \frac{e^2}{|r_i - r_j|} - \sum_{I=1}^{N_{nuc}} \frac{\hbar}{2M} \nabla^2_I + \frac{1}{2}\sum_{I \neq J} \frac{z_I z_J e^2}{|R_I - R_J|} \tag{1}$$

The kinetic energy of electrons, the electron-nuclei interaction, the electron-electron interaction, the kinetic energy of nuclei, and the nuclei-nuclear interaction, respectively, are the five terms in the right-hand side of Eq. (1) where r_i is position of ith electron and R_I is position of Ith nucleus with charge z_I. They assumed the nuclei were at equilibrium and only the electrons were moving because nuclei are heavier than individual electrons. Therefore Eq. (1) can be written in a new form as shown below:

$$\hat{H} = -\sum_{i=1}^{N_e} \frac{\hbar}{2m} \nabla^2 - \sum_{i,I} \frac{z_I e^2}{|r_i - R_I|} + \frac{1}{2}\sum_{i \neq j} \frac{e^2}{|r_i - r_j|} \tag{2}$$

This is the Born-Oppenheimer approximation, which provides an acceptable energy for a basic system but may be insufficient for solving more complex systems.

2.2 The Hohenburg-Kohn Theorem

The Hohenberg-Kohn theorems apply to any system in which electrons move under the influence of a potential. Two theorems made by Hohenberg and Kohn are known to be the DFT's starting point.

Theorem I: There is a one-to-one relation between the external potential and ground state density for the interacting particles system in an external potential.

We can write the ground state wave function as a unique functional of the ground state electron density. As a result, the ground state energy ε can be written as a function of the ground state density, as indicated in Eq. (3)

$$\left\langle \psi[n_0] | \hat{H} | \psi[n_0] \right\rangle = \varepsilon[n_0(r)] \qquad (3)$$

$n_0(r)$ is electron density in a function of electron positions. $\varepsilon[n_0(r)]$ is an energy in a function of density. Although the first Hohenberg–Kohn theorem mathematically shows that an electron density functional exists, it explains nothing about the functional's actual form.

Theorem II: The second Hohenberg–Kohn theorem defines an important property of the functional and states that "the ground state energy can be determined by minimizing total energy, which is a function of electron density by variational principle of the energy functional".

This can be expressed mathematically as seen below.

$$\left. \frac{\delta \varepsilon[n(r)]}{\delta n} \right|_{n=n_0} = 0 \qquad (4)$$

ε_0 is the exact ground state energy which correspond to ground state density $n_0(r)$ by $\varepsilon_0 = \varepsilon[n_0(r)]$

2.3 Self-consistent Kohn-Sham equation

The structural phase transitions can be calculated using Density Functional Theory (DFT), which is an excellent theoretical theory. In this study, DFT was used to examine the structure properties of MgH_2 (FCC), MgH_2 (HCP), MgH_3. The equation derived by Kohn and Sham called the Kohn-Sham equation [14],

$$[\frac{-\nabla^2}{2m} + V_{eff}(r)]\, \psi_n(r) = \varepsilon_n \psi_n(r) \qquad (5)$$

where the effective potential is

$$V_{eff}(r) = V_{ext}(r) + V_H[n(r)] + V_{xc}[n(r)] \qquad (6)$$

$V_{ext}(r)$ is external potential. $V_H[n(r)]$ is Hartree potential. $V_{xc}[n(r)]$ is the exchange correlation potential

with

$$V_H[n(r)] = \int \frac{n(r')}{|r - r'|} dr'$$

and

$$V_{xc}[n(r)] = \frac{\delta E_{xc}[n(r)]}{\delta n}.$$

The first two terms, $V_{ext}(r)$ and $V_H[n(r)]$ can determine from the effective potential, whereas the last term, $V_{xc}[n(r)]$ is still unknown. The exchange correlation potential, $V_{xc}[n(r)]$, contains all quantum mechanical and explicit many-body effects that are unknown. The Local Density Approximation (LDA) and the Generalised Gradient Approximation (GGA) are two types of techniques for general correlation exchange functions [18].

2.3.1 Local Density Approximation (LDA):

It is a type of density functional theory (DFT) approximations to the exchange–correlation energy functional which is certainly based on the electronic density at each position in space. The exchange–correlation energy can be approximated directly using a lot of techniques. The local approximation obtained from the uniform electron gas concept [19], on the other hand, is the most popular. The proposed approximation is thus given by

$$E_{xc}^{LDA}[n(r)] = \int n(r)\epsilon_{xc}^{Hom}[n(r)]dr \qquad (7)$$

where $n(r)$ is the electronic density and ϵ_{xc}^{Hom} is the exchange-correlation energy per particle of a homogeneous electron gas of charge density. However, in many situations, such as in the case of rapidly varying density systems–more complicated systems, it is typically not appropriate to use LDA.

2.3.2 Generalised Gradient Approximation (GGA)

The electron density in most actual situations is unlikely to be uniform, making the LDA method unworkable in many ways. Despite this, many attempts have been made to develop the LDA by taking higher-order exchange-correlation energy components into account. Consequently, not only is the electron density, $n(r)$, included in the exchange-correlation energy, but the gradient of density, $\nabla n(r)$, is also taken into account, which is expressed as

$$E_{xc}^{GGA}[n(r)] = \int n(r)\epsilon_{xc}[n(r), \nabla n(r)]dr \qquad (8)$$

The self-consistent field (SCF) method is an iterative procedure for solve the Kohn-Sham equation to obtain the effective potential, the starting value of the density is first

guessed. The total energies and Kohn-Sham orbitals are then calculated using the equation. The new density is then derived from the Kohn-Sham orbitals that were just calculated and applied to the next phase. This iterative method repeats itself until the density convergence condition is satisfied. Finally, the output quantities, such as band structures and density of states, are calculated using the converged density. Figure 2 shows the complete numerical procedure.
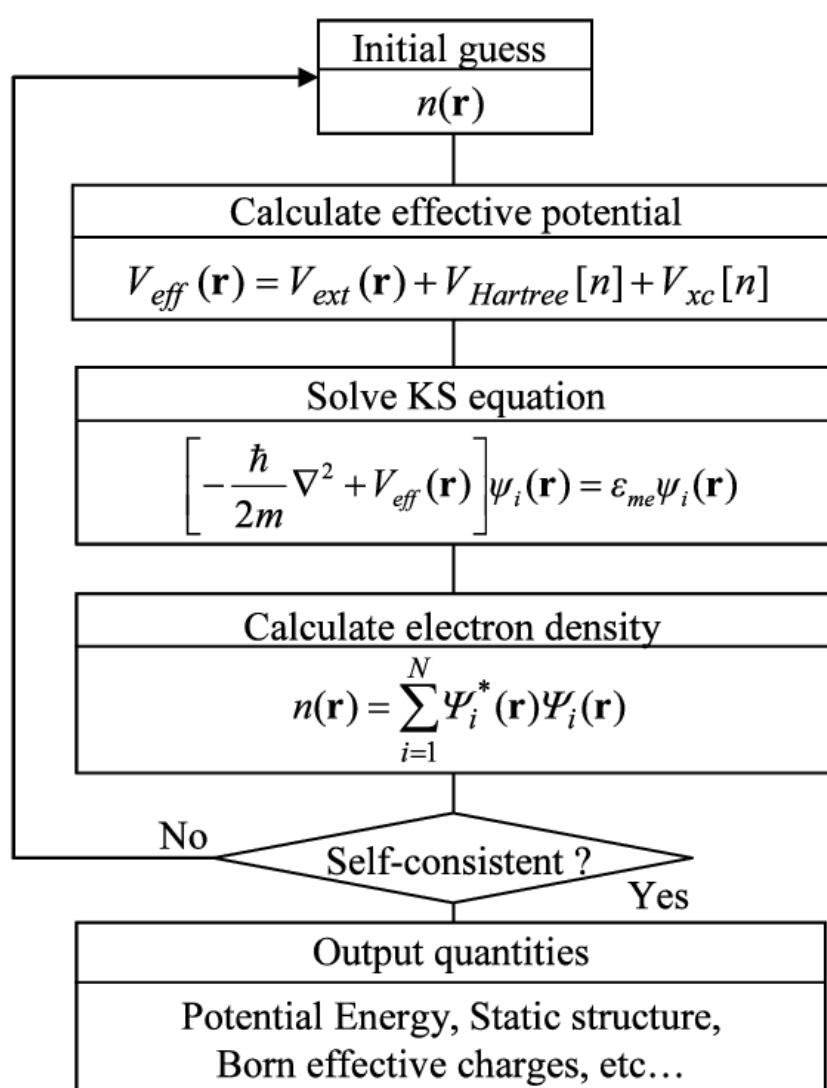
Figure 2 Schematic of the SCF method

2.4 Calculation techniques in DFT
2.4.1 Plane wave basis set

Different types of problems in solids make it difficult to calculate the Kohn-Sham equation for real materials. By considering simply a periodic solid that is invariant under translational and rotational symmetries, the Bloch theorem can be applied to reduce this difficult problem [20] . According to Bloch theorem, the electron wave function is plane waves multiplied by a periodic function $u_k^n(r)$ as solutions of the Schrödinger equation.

$$\psi_k^n(r) = u_k^n(r)\, e^{ik \cdot r} \tag{9}$$

where k is a wave vector and n is a band index. The wave function and energy eigenvalue must satisfy the condition

$$\varepsilon(k) = \varepsilon(k+G) \tag{10}$$

$$\psi_k^n(r) = \psi_{k+G}^n(r) \tag{11}$$

with G being the reciprocal lattice vector. Consequently, the maximum value of G, G_{max} is associated to the kinetic cutoff energy by the expression

$$\varepsilon_{max} = \frac{\hbar^2 G_{max}^2}{2m} \tag{12}$$

As for the periodic function, it's described as a sum of plane wave sets.

$$u_k^n(r) = \sum_j C_j^n(k) e^{iG_j \cdot r} \tag{13}$$

By plugging Eq. (13) into Eq. (9), the volumetric normalized electron wave function is

written as

$$\psi_k^n (r) = \frac{1}{\sqrt{V}} \sum_j C_j^n (k) e^{i(K+G_j) \cdot r} \qquad (14)$$

2.4.2 The pseudopotential method of Projected Augmented Wave

The PAW (Projected Augmented Wave) approach was chosen to be used during whole project. This methodology evolved gradually from the augmented plane wave method with separating the wave function into two parts: partial wave expansions inside of sphere and envelope function from outside sphere [21] . At the sphere boundary, the envelope of function must be differentiable and totally matched. Because there are an infinite number of partial waves near to the atomic core, the all-electron wave function, ψ, transformed into a fictional smooth function known as the auxiliary wave function. $\tilde{\psi}$, containing a smaller amount of partial wave basis. Within the sphere of volume Ω_R, Any wave function, can be distributed as a linear combination of partial wave basis sets, as well as the fictitious smooth wave function.

$$|\psi(r)\rangle = \sum_i a_i |\phi_i(r)\rangle \text{ , inside } \Omega_R \text{ and} \qquad (15)$$

$$|\tilde{\psi}(r)\rangle = \sum_i b_i |\tilde{\phi}_i(r)\rangle \text{ , inside } \Omega_R \qquad (16)$$

whereas the all-electron partial wave and the auxiliary partial wave outside the sphere are

identical:

$$\phi_i(r) = \tilde{\phi}_i(r) \text{ , outside } \Omega_R \qquad (17)$$

The all-electron partial wave is the solution to the radial Schrödinger equation for an isolated atom, and the auxiliary wave function may be chosen from the all-electron partial wave that matches the all-electron partial wave outside of the sphere. As a result, the transformation operator, relates the additional wave function and the all-electron wave function.

$$|\psi\rangle = \tau|\tilde{\psi}\rangle \qquad (18)$$

the transformation operator can be defined as follows

$$\tau = \hat{1} + \sum_R S_R \qquad (19)$$

The transformation operator is frequently done by adding the identity operator with the sum of the atomic contributions at each specific site R as described in Eq (19). The atomic contribution reflects the difference between the all-electron partial wave and the auxiliary partial wave. Which is

$$S_R|\tilde{\phi}_i\rangle = |\phi_i\rangle - |\tilde{\phi}_i\rangle \qquad (20)$$

The new operator $|\tilde{P}_i\rangle$ described as the projection operator in atomic space that represents the local character of a wave function [22]. The partial wave basis set must be orthonormal to the operator.

$$\langle\tilde{P}_m|\tilde{\phi}_n\rangle = \delta_{mn} \qquad (21)$$

By using the mentioned property, the smooth wave function can be written as

$$|\tilde{\psi}\rangle = \sum_i |\tilde{\phi}_i\rangle\langle\tilde{P}_i|\tilde{\psi}\rangle \qquad (22)$$

By applying Eq. (19) into (22), we have

$$|\psi\rangle = \left(\hat{1} + \sum_i(|\phi_i\rangle - |\tilde{\phi}_i\rangle)\langle\tilde{P}_i|\right)|\psi\rangle. \qquad (23)$$

With the transformation operator which can write as

$$\tau = \hat{1} + \sum_i(|\phi_i\rangle - |\tilde{\phi}_i\rangle)\langle\tilde{P}_i|. \qquad (24)$$

the expected value of an arbitrary operator denoted by A:

$$\langle A\rangle = \sum_n f_n\langle\psi_n|A|\psi_n\rangle$$

$$= \sum_n f_n \langle \psi_n | \tau^\dagger A \tau | \psi_n \rangle \tag{25}$$

f_n is the occupation number.

$$(\widehat{H} - \varepsilon \tilde{S}) \, |\tilde{\psi}\rangle = 0 \tag{26}$$

this equation can apply the PAW method to the Kohn-Sham equation.

$$\widehat{H} = \tau^\dagger H \tau \tag{27}$$

$$\tilde{S} = \tau^\dagger \tau \tag{28}$$

$\widehat{H}$ is Hamiltonian matrix, $\widehat{H} = \tilde{T} + \tilde{V}$.

2.4.3 The cutoff energy and k-point mesh

The reciprocate space, also known as k-space, presents the Fourier transform of the repeated periodic lattice in real space. The Kohn-Sham equation is solved in reciprocal space with plane waves as basis sets in this research. Equation (14) yields a concrete answer to the Kohn-Sham equation since there are an infinite number of plane-wave basis sets. However, due to a shortage of processing resources, analyzing the exact answer is difficult. As a result, Monkhorst and Pack still provide a limited but useful number of plane-wave basis sets [23], which is influenced by the kinetic cutoff energy, E_{cut}, which is represented by the highest value of the reciprocal lattice vector, G_{max}. The kinetic energy cutoff is now expressed as

$$E_{cut} \leq \frac{\hbar^2}{2m} |k + G_{max}|^2 \tag{29}$$

The more kinetic cutoff energies and k-points there are, the more correctly the energy is calculated; however, it also demands more processing resources.

2.4.4 The geometry optimization

In computational physics, the Hartree–Fock (HF) technique is an approximation approach for determining a quantum many-body system's wave function and energy in a stationary state. The Hartree-Fock method attempts to estimate the solution of the electronic Schrödinger equation, assuming that the wavefunction can be approximated by a single Slater determinant consisting of one spin orbital per electron. In either case, note that the solutions depend on the orbitals. The Hartree-Fock equations can be solved numerically or they can be solved in the space spanned by a set of basis functions (Hartree-Fock-Roothan equations) [24]. As a result, we must first guess some initial orbitals before iteratively refining our guesses. Because of this, Hartree-Fock is known as a self-consistent-field (SCF) method. The Hartree-Fock equations can be defined as follows

$$f(x_1)\chi_i(x_1) = \epsilon_i\chi_i(x_1). \quad (30)$$

where ϵ_i is the energy eigenvalue associated with orbital χ_i. The Hartree-Fock equations are transformed into Roothaan equations by using a basis set. $\tilde{\chi}$ is the atomic orbital basis functions, we have the expansion

$$\chi_i(x_1) = \sum_{\mu=1}^{K} C_{\mu i}\tilde{\chi}_\mu \quad (31)$$

for each spin orbital i. It then leads into

$$f(x_1)\sum_v C_{vi}\tilde{\chi}_v(x_1) = \epsilon_i \sum_v C_{vi}\tilde{\chi}_v(x_1). \quad (32)$$

A matrix equation is obtained by multiplying $\chi_\mu^*(x_1)$ on the left-hand side and integrating.

$$\sum_\nu C_{\nu i} \int dx_1 \, \chi_\mu^*(x_1) f(x_1) \tilde{\chi}_\nu(x_1) =$$
$$\epsilon_i \sum_\nu C_{\nu i} \int dx_1 \, \chi_\mu^*(x_1) \tilde{\chi}_\nu(x_1). \text{ (33)}$$

This could be greatly simplified by using matrix element notation.

$$S_{\mu\nu} = \int dx_1 \, \chi_\mu^*(x_1) \tilde{\chi}_\nu(x_1), \text{ (34)}$$

$$F_{\mu\nu} = \int dx_1 \, \chi_\mu^*(x_1) f(x_1) \tilde{\chi}_\nu(x_1). \text{ (35)}$$

The Hartree-Fock-Roothaan equations can now be expressed as a matrix:

$$\sum_\nu F_{\mu\nu} C_{\nu i} = \epsilon_i \sum_\nu S_{\mu\nu} C_{\nu i} \text{ (36)}$$

or

$$FC = SC\epsilon \text{ (37)}$$

where ϵ_i is the orbital energy that is represented by a diagonal matrix ϵ. Except for the overlap matrix S, this is an eigenvalue equationTo make S disappear, one must perform a basis transformation to an orthogonal basis, after which an eigenvalue equation can be solved. Because F is depend on its own solution (via the orbitals), the method must be repeated iteratively. This is why the solution of the Hartree-Fock-Roothaan equations are often called the self-consistent-field method.

The process of arranging crystal structures in space so that their energies are minimized is known as geometry optimization. The investigated structure is relaxed to the point where each atom's net interatomic force is as close to zero as possible, and the atomic positions stay constant. In DFT, however, the temperature is ignored; the system in contact with any pressure value and T= 0 K reservoirs prefer the minimum enthalpy.

$$H = E + PV \qquad (38)$$

Enthalpy is the sum of the internal energy and pressure times volume. The matrix of lattice vector $h = \{a, b, c\}$ and the coordinate $s_i, i = 1 \ldots N$ use to examine the crystal structure by relate to h of N atoms in unit cell and $V = \det(h)$. We use the finite strain tensor as a free variable instead of the lattice vectors since the energy per unit cell is a function of h and s_i. The strain components have 9 dimensions and 3N, the enthalpy now has a functional of (9 + 3N)-dimensional space [25].

$$H = H(\epsilon, r_1, r_2, r_3, \ldots, r_n) \qquad (39)$$

The force component is created by taking the first derivative of the enthalpy with respect to the coordinates of atoms X_i.

$$F = -\frac{\partial H}{\partial X_i}\bigg|_P \qquad (40)$$

Around the lowest X_{min}, the enthalpy variation is defined as

$$\delta H = \frac{1}{2}(X - X_{min}) \cdot B(X - X_{min}) \qquad (41)$$

The Hessian matrix is denoted by B. The technique of quasi-Newton is being used to reduce lattice parameters. The searching for the X_{min} from the force for one relaxation step is aided by the internal coordinates of pressured crystals [25]. The X_k is written as

$$\Delta X_k = H_k F_k \qquad (42)$$

and

$$H = B^{-1}$$

Despite H_0 being unidentified. The crystal structure eventually fulfills the external pressure criterion and also has the smallest enthalpy, as determined by the algorithm, when X reaches its minimum.

2.4.5 Electronic band structure

The electronic band structure (or simply band structure) of a material in solid-state physics explains the range of energy levels that electrons can have within it, as well as the ranges of energy levels that they can't have. The ground-state wave function is given by the Kohn-Sham equation solution, Eq. (5), which also relates to the system's Hamiltonian. The system's electrical characteristics are then determined by computing the expected values of the total energy responsible for each k-vector. Which is obtained by

$$\langle \psi_{nk\prime} | \hat{H} | \psi_{nk} \rangle = \epsilon_{nk} \delta_{kk\prime} \qquad (43)$$

The electronic band structure is produced by displaying the set of eigenvalues along the high symmetry points over the first Brillouin zone after getting energies matching each value of the wave vector k. When identifying if a crystal is an insulator, conductor,

or semiconductor, the band structure can be examined. The band gap between the valence and conduction bands is seen in figure 3. If the crystal is a conductor, the conduction and valence bands will overlap, which means there is no band gap. The crystal is a semiconductor when the energy gap between the conduction band and the valence band is more than 0 and less than 3 eV. The energy gap between valence bands and conduction band is too large for the electron to make the jump to escape from its atom and be promoted to the valance band in insulators with a band gap greater than 3 eV[26].
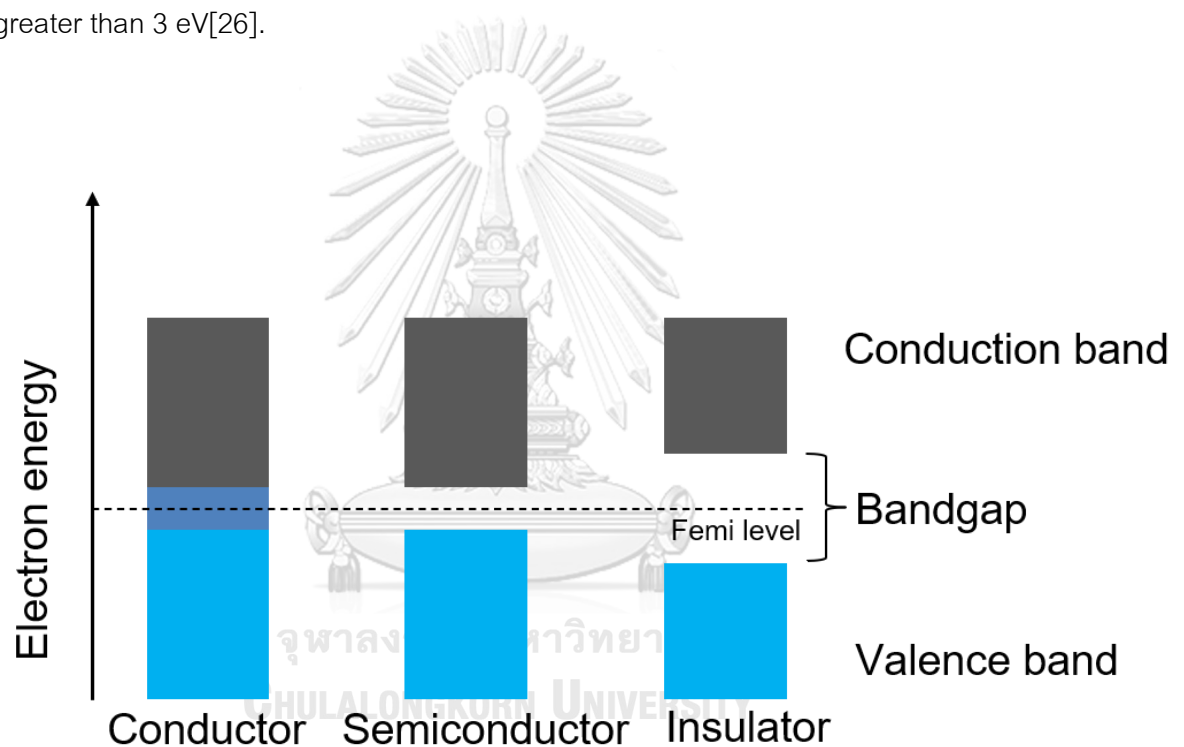
Figure 3 The energy band gap of conductor, semiconductor and insulator

By increasing the pressure to the crystal, the gap between the conduction and valence bands can be changed. An insulator's valence band is completely filled with electrons. The gap will close after applying pressure to the crystal, and some electrons flow to the conduction band, making the crystal metal.

2.4.6 Density of states

The quantity of all electrons permitted to occupy a specified level of energy is defined as the total density of states. A probability density function is used to represent it mathematically as a distribution. The DOS of nth-energy level is expressed as

$$g(\varepsilon) = \int \delta\big(\varepsilon - \varepsilon_n(k)\big) \tag{44}$$

when the integral is spread over the primitive cell. The energy eigenvalue accounting for the nth-energy level is $\varepsilon_n(k)$. As a result, the partial density of states (PDOS) is defined as the projection of each given atom's orbital onto the density of states.

2.4.7 Phonon's calculation

Based on DFT calculations at 0 K, MgH_2 and MgH_3 structural tests under high pressure were identified in this work. Although, DFT calculations show good agreement with the experimental results in many situations, it cannot clearly prove the unique high-pressure phase. In generally, crystal stability can be explained using phonon frequencies caused by lattice dynamics. As a result, phonon calculations were used to verify the enthalpy-pressure relationship's result. In the structure steady state coordinates, the expansion must be done for the whole energy [27] , which are

$$E = E_0 + \sum_{k,\alpha} \frac{\partial E}{\partial \vec{u}_{k,\alpha}} \cdot \vec{u}_{k,\alpha} + \frac{1}{2}\sum_{k,\alpha,k',\alpha'} \vec{u}_{k,\alpha} \cdot \Phi_{\alpha,\alpha'}^{k,k'} \cdot \vec{u}_{k',\alpha'} + \cdots \tag{45}$$

The force which acts on atom can calculate as following

$$F_{k,\alpha} = \frac{\partial E}{\partial \vec{u}_{k,\alpha}} \tag{46}$$

The force term is zero at equilibrium. The 3rd harmonic approximation and the higher order terms believed to be irrelevant. $\vec{u}_{k,\alpha}$ is the vector of atomic displacements from equilibrium position. $\Phi_{\alpha,\alpha'}^{k,k'}$ is the force constant matrix, which is

$$\Phi_{\alpha,\alpha'}^{k,k'} = \frac{\partial^2 E}{\partial \vec{u}_{k,\alpha} \partial \vec{u}_{k',\alpha'}} \tag{47}$$

DFT calculations are used to compute the force component. Then apply it to Newton's equation of motion to get the matrix eigenvalue equation, which is

$$D\varepsilon_m = \omega_m^2 \varepsilon_m \tag{48}$$

The dynamical matrix is

$$D_{\alpha,\alpha'}^{k,k'}(\vec{q}) = \frac{1}{\sqrt{M_k M_{k'}}} \Phi_{\alpha,\alpha'}^{k,k'} \tag{49}$$

The phonon calculation result can be obtained from eigenvalue, ω_m^2, This explains the frequency dispersion relationship of the structure. The square root of the eigenvalues of the dynamical matrix is used to calculate phonon frequencies. Because these eigenvalues can be positive or negative, phonon frequencies can be positive real or imaginary numbers. In Quantum-ESPRESSO code produce negative values at imaginary frequencies so If the phonon frequency is positive, the structure will be stable. If the phonon frequency is negative, the structure will be instability.

2.4.8 Isotope effect

The replacement of an atom by one of its isotopes has proven to be very useful in the study of reaction mechanisms. The discovery of the isotope effect in ordinary superconductors was essential in the development of the Bardeen-Cooper-Schrieffer (BCS) theory, Cooper pairs are formed by electrons interacting through lattice vibrations

[28]. For example, the expression on the isotope coefficient (α) for H₃S superconductor [29] in the function of the pressure was

$$\alpha = \frac{\omega_{ln} dT_c}{2T_c d\omega_{ln}} \qquad (50)$$

The electron-phonon pairing kernel has the following form

$$K(z) = 2 \int_0^{+\infty} d\Omega \frac{\Omega \bar{\alpha}^2(\Omega)F(\Omega)}{\Omega^2 - z^2} \qquad (51)$$

Where $\bar{\alpha}^2(\Omega)F(\Omega)$ is The Eliashberg functions [30]. In the Eliashberg formalism, the depairing electron correlations are expressed by the the following:

$$\mu^*(\omega_n) = \mu^* \theta(\omega_c - |\omega_n|) \qquad (52)$$

$$\omega_c = 3\Omega_{max} \qquad (53)$$

μ^* is the Coulomb pseudopotential. Ω_{max} is the Debye frequency. θ is the Heaviside function. ω_c is the cut-off frequency

The Coulomb pseudopotential was defined by Morel and Anderson [31].

$$\mu^* = \frac{\mu}{1 + \mu \ln\left(\frac{\omega e}{\omega_{ln}}\right)} \qquad (54)$$

ω_e is the characteristic electron frequency. Logarithmic phonon frequency ω_{ln} is expressed by

$$\omega_{ln} = \exp\left[\frac{2}{\lambda} \int_0^{\Omega_{max}} d\Omega \frac{\bar{\alpha}^2(\Omega)F(\Omega)}{\Omega} \ln(\Omega)\right] \qquad (55)$$

$$K_B T_c = \omega_{ln} exp\left[\frac{-(1+\lambda)}{(\lambda - \mu^*(1 + 0.4747\lambda))}\right] \qquad (56)$$

The electron-phonon coupling constant λ is derived from

$$\lambda = 2 \int_0^{\Omega_{max}} d\Omega \, \frac{\bar{\alpha}^2(\Omega)F(\Omega)}{\Omega} \qquad (57)$$

Thus

$$\alpha = \frac{1}{2}\left[1 - \frac{(1+\lambda)(1+0.4747\lambda)(\mu^*)^2}{(\lambda-\mu^*(1+0.4747\lambda))^2}\right] \qquad (58)$$

For superconducting material, the critical temperature is inversely proportional to square root of isotopic mass M

$$T_c = \frac{1}{M^\alpha} \qquad (59)$$

$$T_c = \frac{1}{\sqrt{M}}, \alpha = 0.5 \qquad (60)$$

จุฬาลงกรณ์มหาวิทยาลัย
CHULALONGKORN UNIVERSITY

3. CALCULATION DETAILS

In this work, we calculated the structures of MgH_2, MgH_2 (HCP), MgH_3 under pressure between 0-300 GPa in order to determine the formation enthalpy and electronic property of their structures under high pressure by using density functional theory (DFT) which were numerically calculated. We also substituted the hydrogen atoms with deuterium (D) to determine the dynamical stability under high pressure. The total energy was to be reported and applied to examine the electronic band structures, DOS and phonon dispersion.

3.1 Structure

In this work MgH_2 (FCC), MgH_2 (HCP), MgH_3 structures in figures 4, 5 and 6 were chosen as models to find stable structures under high pressure to be used as a basic model for calculating the critical temperature in the future work.

Table 1. Lattice parameters of MgH_2 (FCC), MgH_2 (HCP), MgH_3 at the atmospheric pressure (0 GPa).

Structure	Space group	a (Å)	b (Å)	c (Å)	Density (g/cm^3)	Volume $(Å^3)$
MgH_2	Fm-3m	3.367	3.367	3.367	1.62	26.999
MgH_2	P6/mmm	3.074	3.074	3.534	2.64	28.917
MgH_3	Fm-3m	3.327	3.327	3.327	1.74	26.042
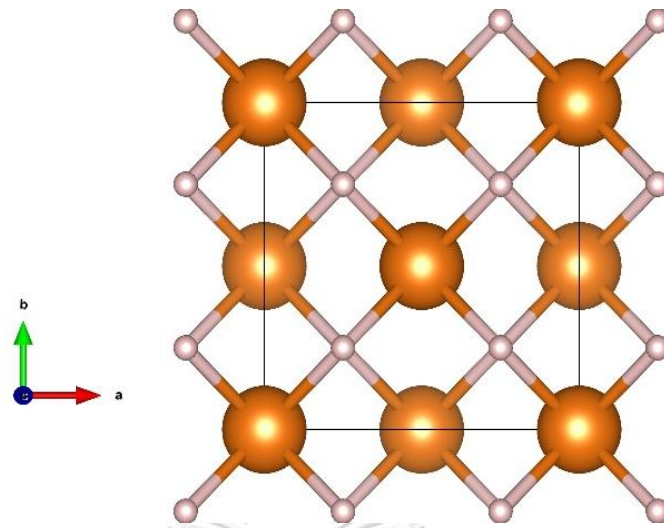
Figure 4 The Fm-3m structure of MgH$_2$ or the face centered cubic
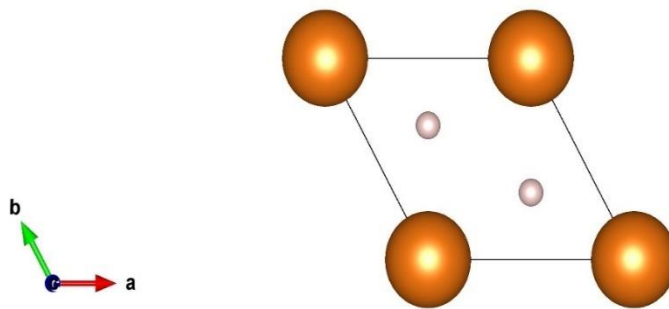
Figure 5 The P6/mmm structure of MgH$_2$ or hexagonal close packed
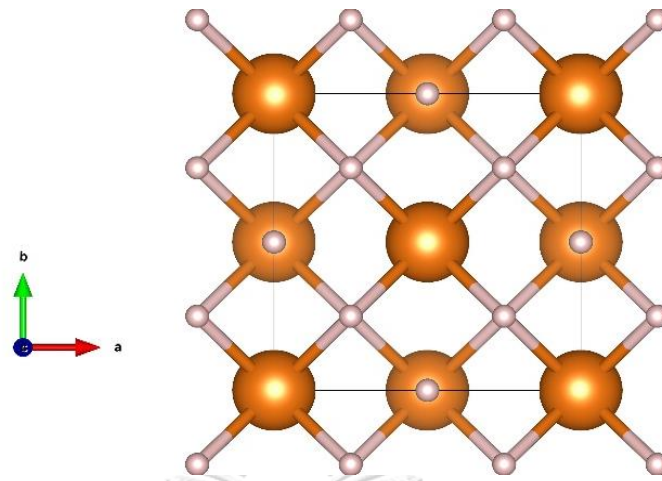
Figure 6 The Fm-3m structure of MgH_3 or the face centered cubic

Quantum Espresso Package [15] was used to examine the physical characteristics of MgH_2, MgH_2 (HCP), MgH_3 and substituted the hydrogen atoms with deuterium (D). The pseudopotentials for the core and valence electrons were described using the projector augmented wave technique (PAW) [32] . We used the Perdew-Burke-Ernzerhof (PBE) functional for the generalized gradient approximation (GGA). The convergence test needs to be achieved systematically to accurately assessed physical quantities with the aid of DFT.

3.2 Convergence test

Convergence tests are crucial for determining the correctness of the system's total ground-state energy. A convergence test is a method of improving the input script for a simulation in order to make optimum use of limited computer resources. To determine the simulation's accuracy and dependability, it's important to identify an optimal initial setting for study. The kinetic cutoff energies and k-point meshes are the parameters that must be optimized. Convergence test is a technique of increasing the effectiveness of limited computer resources by optimizing the input script for a simulation. To determine the simulation's correctness and reliability, it's important to identify a suitable setup for research for a certain system. Convergence testing of the MgH_2(FCC) structure can be

divided into 2 parts. The k-point mesh of 4 x 4 x 4 was chosen and kept as a fixed value, after which the cutoff energies ranging from 30 to 120 Ry were varied, and each of the calculated total energies corresponding to each of the cutoff energies was plotted in Figure 7. The energies immediately decrease during the cutoffs from 30 to 120 Ry, as shown in Figure 7.
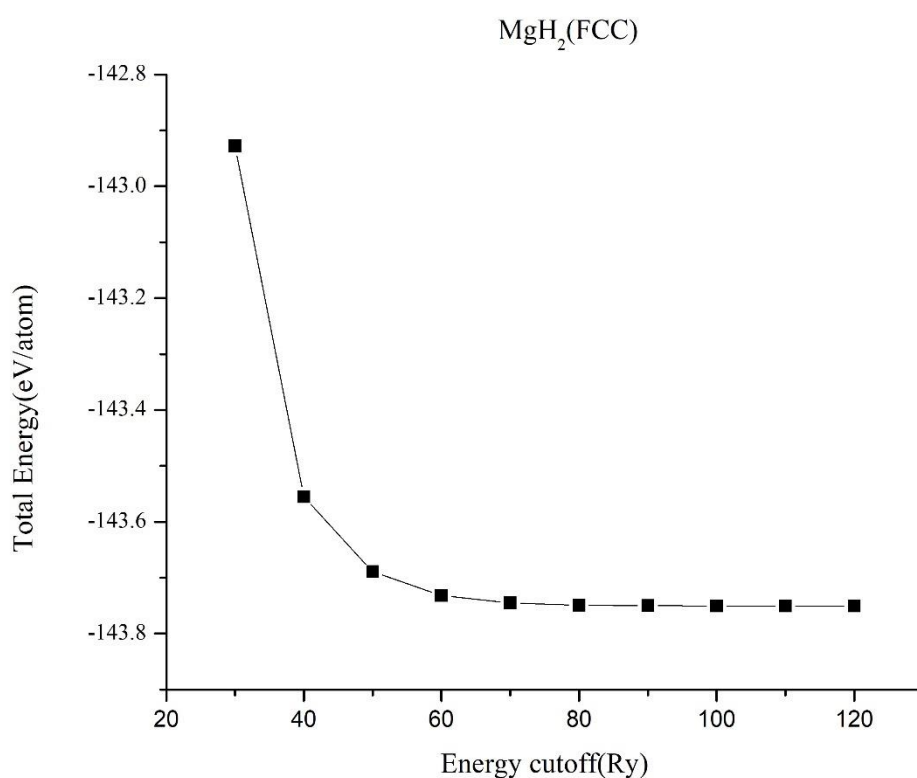
Figure 7 The convergence test of total energy with the energy cutoff for FCC in MgH_2

The cutoff energy of 80 Ry was chosen for the remainder of the calculations because when the cutoff is larger, the difference in calculating the total energy of this system is even smaller. The difference between cutoff energies of 80 and 90 Ry is less than 0.01 eV, which is technically acceptable.
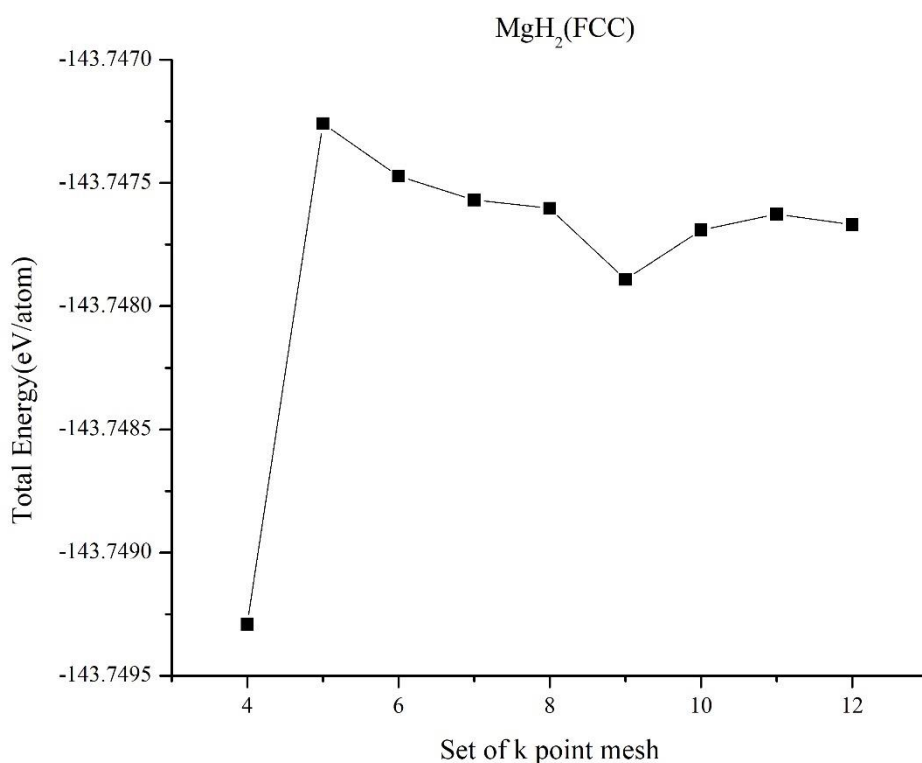
Figure 8 The convergence test of total energy with the k point mesh for FCC in MgH_2

In the second part, the cutoff energy of 80 Ry was chosen and kept as a constant value, after which the set of k-point from 4 x 4 x 4 to 12 x 12 x 12 were varied and plotted in figure 8. The energy curve fluctuates a little initially, but it tends to stabilize at 11 x 11 x 11. The set of k-point $11 \times 11 \times 11$ and $12 \times 12 \times 12$ has the total energy difference less than 0.0001 eV, so thus the k-point of $12 \times 12 \times 12$ was chosen. Other physical properties of the MgH_2(FCC) structure were calculated using the cutoff energy of 80 Ry and the k-point mesh of 12 x 12 x 12 as input parameters.

The same processes are used in the MgH$_2$(HCP) convergence test in figure 9, with the k-point 4 x 4 x 4 kept as a fixed parameter, and the cutoff energies ranging from 40 to 120 Ry. During the cutoffs from 40 to 120 Ry, the total energies decrease. Because the difference in cutoff energies between 80 and 90 Ry is less than 0.01 eV, the 80 Ry cutoff energy was chosen to be the same as MgH$_2$ (FCC).
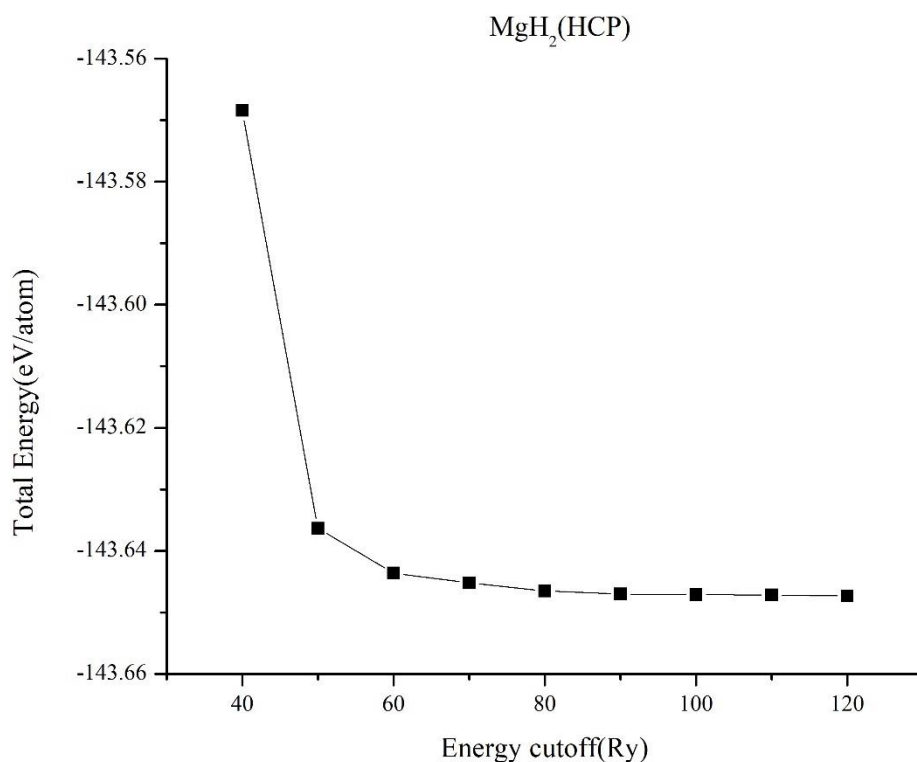
Figure 9 The convergence test of total energy with the energy cutoff for HCP in MgH$_2$

The second procedure is the k point test, which uses an 80 Ry cutoff energy as a fixed parameter, followed by the k-point meshes test from 4 x 4 x 2 to 12 x 12 x 2 in figure 10. The results revealed that the obtained energy fluctuates. As a result, additional tests were carried out to assess the total energy's stability.
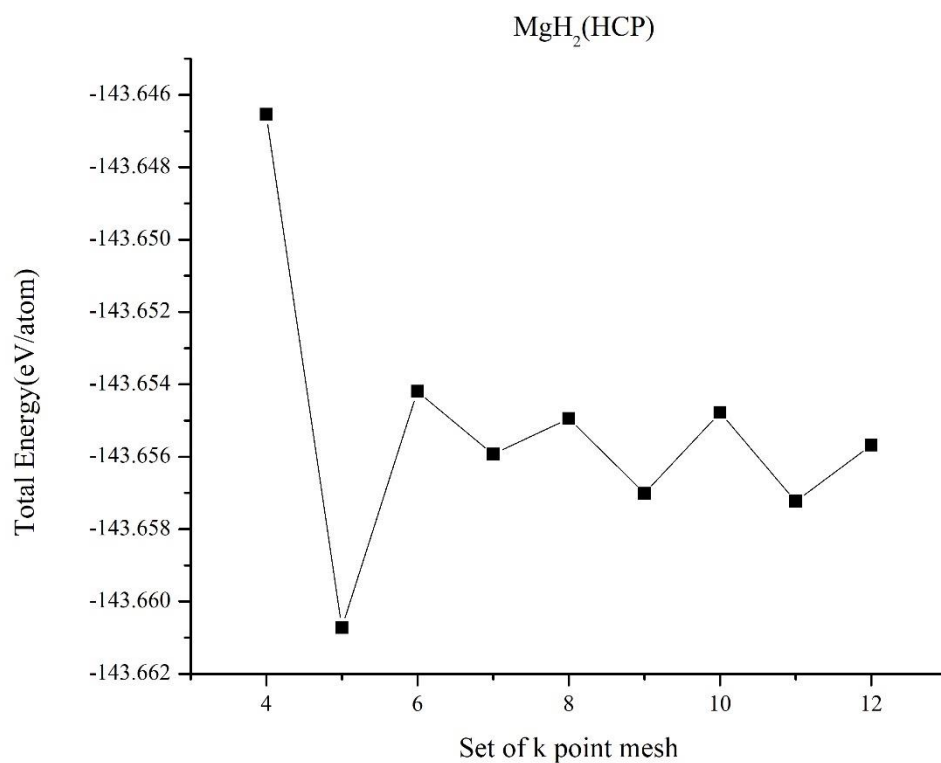
Figure 10 The convergence test of total energy and the k point set for HCP in MgH_2 (n x n x 2)

In figure 11 the first two k values were set to 12 by the test, which ranged from 12 x 12 x 2 to 12 x 12 x11. The findings revealed that the difference in energy between the k-point meshes of 12 x 12 x 8 and 12 x 12 x 9 is less than 0.0001 eV, therefore the 12 x 12 x 8 k-point mesh was chosen. In order to calculate the structure of MgH_2 (HCP), the cutoff energy of 80 Ry and the k-point mesh of 12 x12 x 8 were utilized as input parameters.

MgH$_2$(HCP)
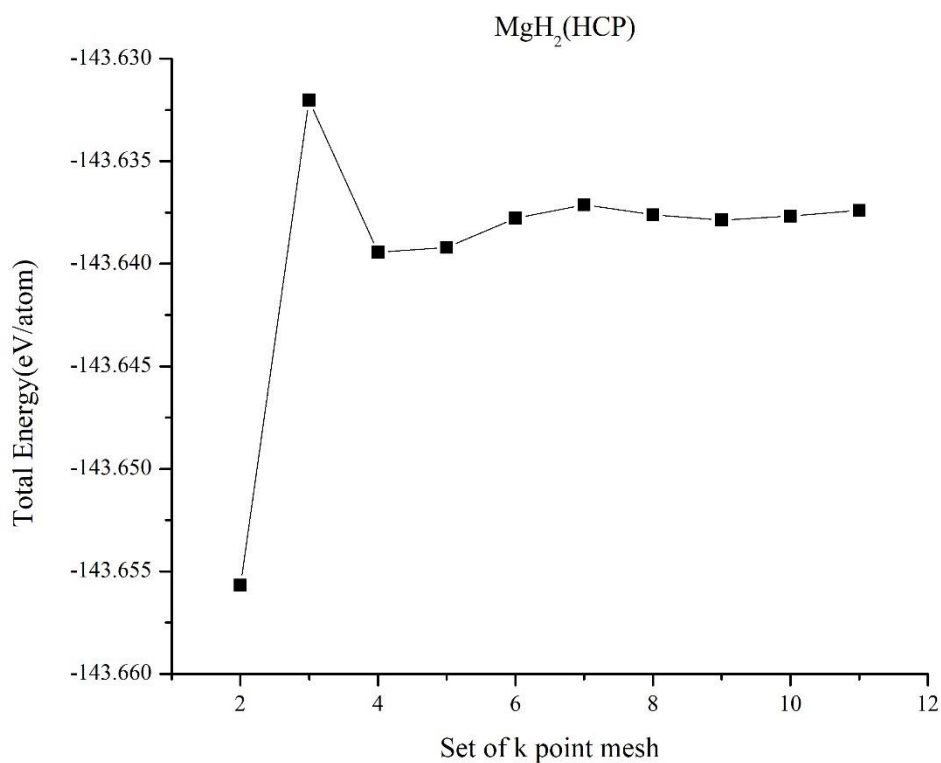
Figure 11 The convergence test of total energy and the k point set for HCP in MgH$_2$ (12 x 12 x n)
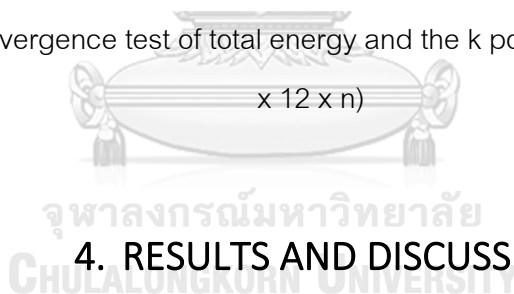
4. RESULTS AND DISCUSSIONS

4.1 The convex hull of Mg–H system

This section carefully describes all processes within this work as follows: First, we calculate the enthalpy of MgH$_2$ and MgH$_3$ at 0-300 GPa then simulate the structure of pure hydrogen (HCP, monoclinic) and pure magnesium (HCP, BCC) to determine the enthalpy at pressure 0-300 GPa for calculate the enthalpy difference of MgH$_2$, MgH$_3$ to find the convex hull curve comparing with the enthalpy difference between Mg and H. The hydrogen phases that use in the calculation are P6$_3$/m at 0 – 50 GPa and C2/c at

100-300 GPa [33]. We calculated the formation enthalpy of $Mg_{1-x}H_x$ using a fractional representation of $Mg_{1-x}H_x$ with respect to its decomposition into Mg and H as

$$\Delta H(Mg_{1-x}H_x) = H(Mg_{1-x}H_x) - [(1-x) \times H(Mg) + x \times H(H)]$$

where x is the concentration of H. The formation enthalpies from 0 to 300 GPa were evaluated as the difference in the enthalpy of the predicted Mg–H system.
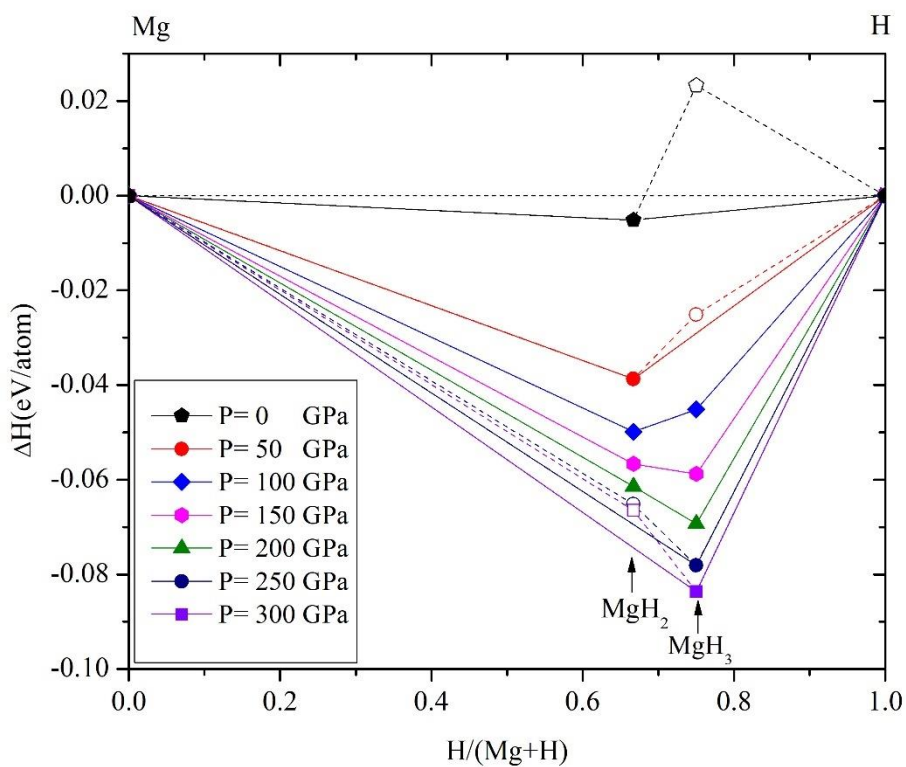
Figure 12 The enthalpy per atom of MgH$_2$ (FCC) and MgH$_3$ (FCC) are presented in the form of the convex hull (solid markers refer to a stable structure, whereas transparent markers refer to a meta-stable structure)

The convex hulls in figure 12 showed that the Fm-3m structure of MgH_3 is thermodynamically stable between 100–300 GPa and 0–200 GPa for MgH_2. Moreover, at 150 GPa and above, MgH_3 becomes more energetically favorable than MgH_2. The D atoms were also used instead of the H atoms. Despite this, the enthalpies per atom of MgH_x and MgD_x are exactly equivalent because the pseudopotentials are identical; the only difference is the masses of H and D. Structures that exist on the convex hull are either thermodynamically stable or meta-stable and can be synthesized in principle. From the results we can find the calculation of electronic band structure, density of states and phonon dispersion of stable structures from the convex hull.
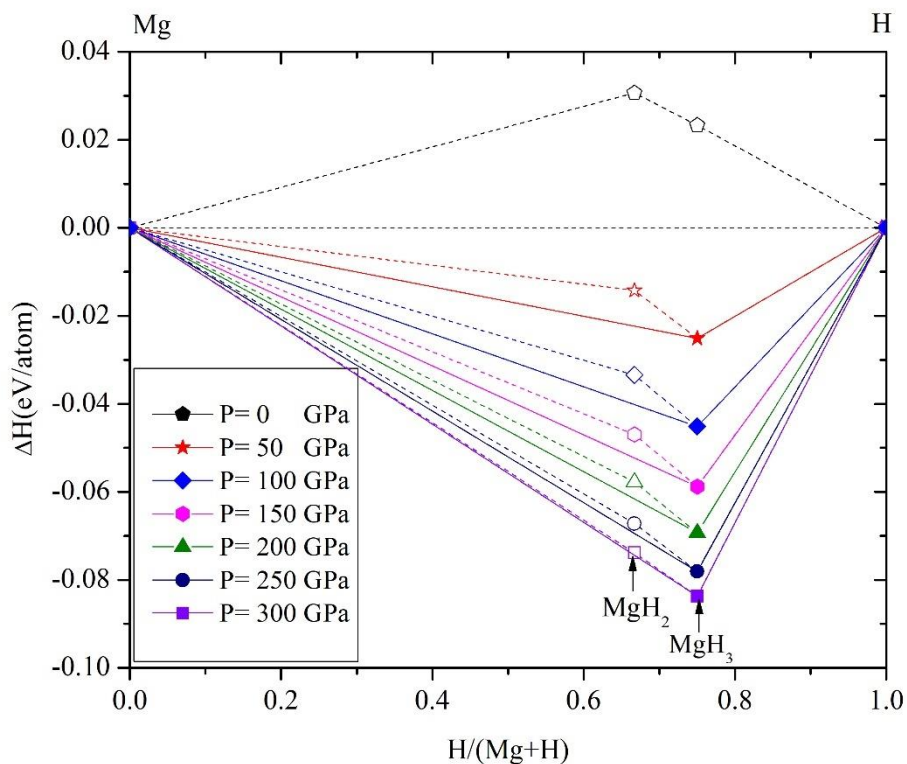
Figure 13 The enthalpy per atom of MgH_2 (HCP) and MgH_3 (FCC) are presented in the form of the convex hull (solid markers refer to a stable structure, whereas transparent markers refer to a meta-stable structure)

However, the convex hulls of MgH_2 (HCP) and MgH_3 (FCC) in figure 13 show that the enthalpies per atom of the MgH_2 (HCP) structure are unstable at every pressure. As a result, we decided not to look into the structure's electronic band structure, density of states, or phonon dispersion calculations. Therefore, there are 4 types of structural examination remaining in this project which are MgH_2 (FCC), MgH_3 (FCC), MgD_2 (FCC) and MgD_3 (FCC).

4.2 The phonon dispersion

Due to the finite size of the simulated material system, the first Brillouin zone is frequently sampled with a set of discrete k points in computational works. A k point represents a point in the reciprocal space, similar to a R point, which represents a point in the direct space. The first Brillouin zone is necessary for studying crystals' electrical, thermal, and optical properties. The first Brillouin zone of FCC crystals is seen in figure 14.
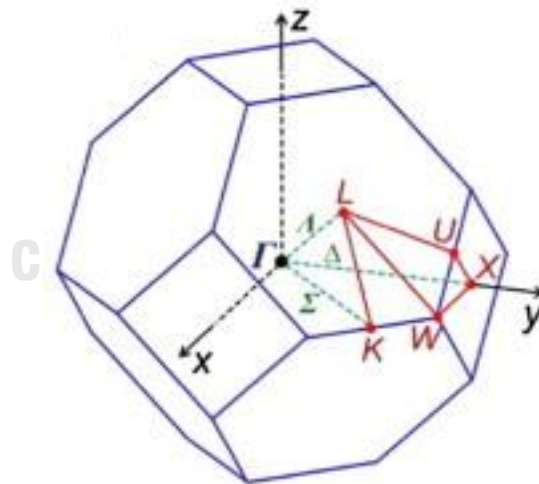
Figure 14 The FCC lattice's first Brillouin zone, which includes the high symmetry k points and directions [34]

Table 1. The first Brillouin zone of an fcc lattice. $\vec{k} = u\vec{b}_1 + v\vec{b}_2 + w\vec{b}_3$

Symmetry points (u, v, w)	$[k_x, k_y, k_z]$	Description
Γ:(0,0,0)	[0,0,0]	Center of the Brillouin zone
X: (0,1/2,1/2)	[0,2π/a,0]	Center of a square face
L: (1/2,1/2,1/2)	[π/a,π/a,π/a]	Center of a hexagonal face
W: (1/4,3/4,1/2)	[π/a,2π/a,0]	Corner point
U: (1/4,5/8,5/8)	[π/2a,2π/a,π/2a]	Middle of an edge joining a hexagonal and a square face
K: (3/8,3/4,3/8)	[3π/2a,3π/2a,0]	Middle of an edge joining two hexagonal faces

The real space and reciprocal space primitive translation vectors are:

$$\vec{a}_1 = \frac{a}{2}(\hat{x} + \hat{z}), \vec{a}_2 = \frac{a}{2}(\hat{x} + \hat{y}), \vec{a}_3 = \frac{a}{2}(\hat{y} + \hat{z}),$$

$$\vec{b}_1 = \frac{2\pi}{a}(\hat{k}_x - \hat{k}_y + \hat{k}_z), \vec{b}_2 = \frac{2\pi}{a}(\hat{k}_x + \hat{k}_y - \hat{k}_z),$$

$$\vec{b}_3 = \frac{2\pi}{a}(-\hat{k}_x + \hat{k}_y + \hat{k}_z)$$

In the process of calculating the phonon frequency, we tested the MgH_2 and MgD_2 structure at 0 GPa as shown in figure 15 and 16 with the first Brillouin zone W-L-G-X-W-K.
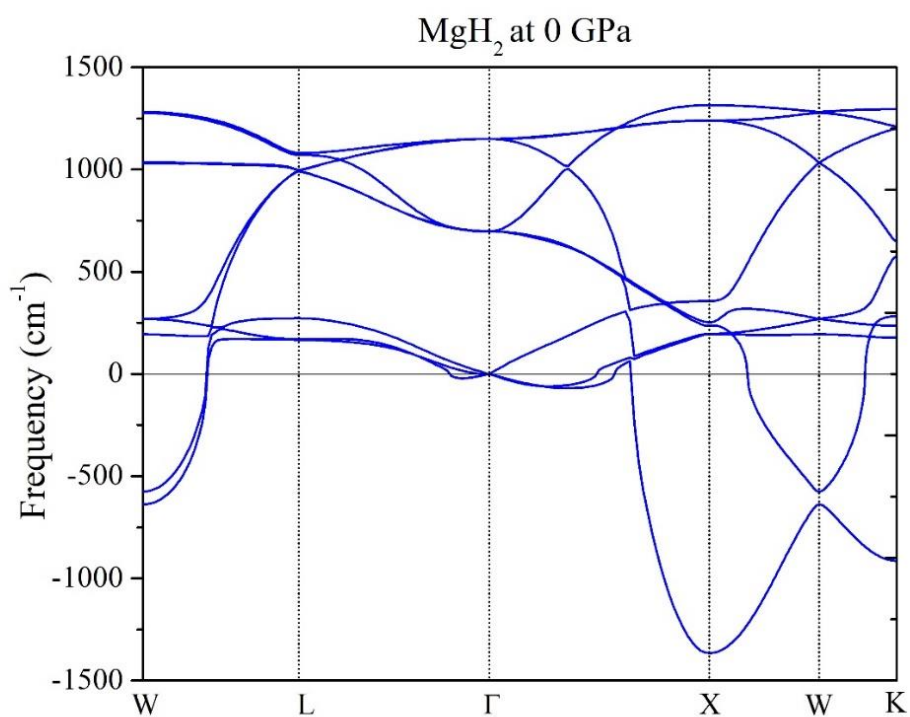
Figure 15 Phonon dispersion of MgH$_2$ at 0 GPa
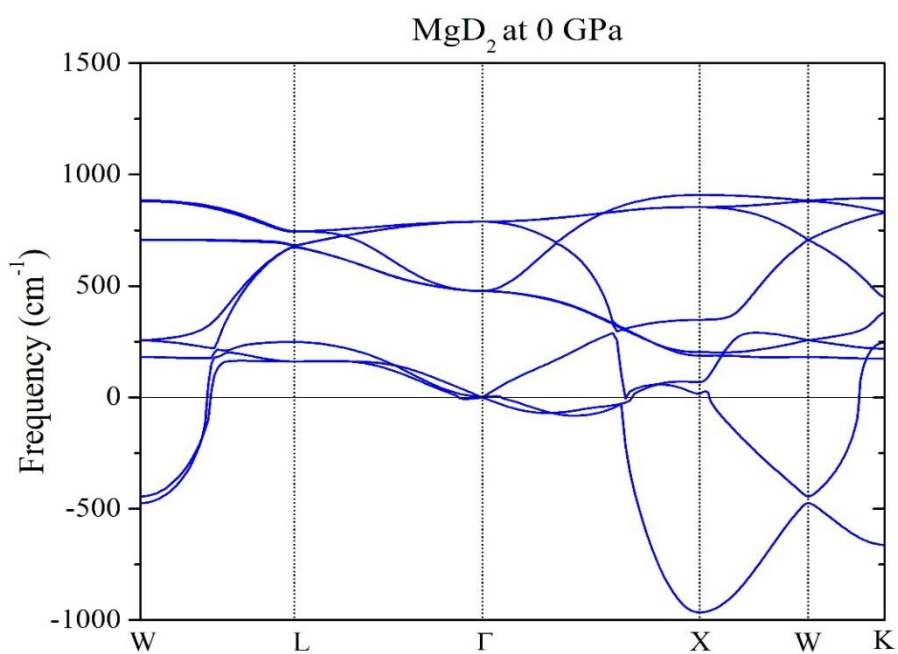
Figure 16 Phonon dispersion of MgD$_2$ at 0 GPa

The results showed that the phonon frequencies of MgH_2 and MgD_2 at 0 GPa did not match the predictions, indicating that the structure was unstable. In the calculations, there are two forms of phonons that are acoustic phonons and optical phonons. In general, acoustic phonons usually converge to zero at the center of the Brillouin Zone and optical phonons exhibit non-zero frequency at the Brillouin Zone center. The frequency of the MgH_2 structure is higher than that of the MgD_2 structure.
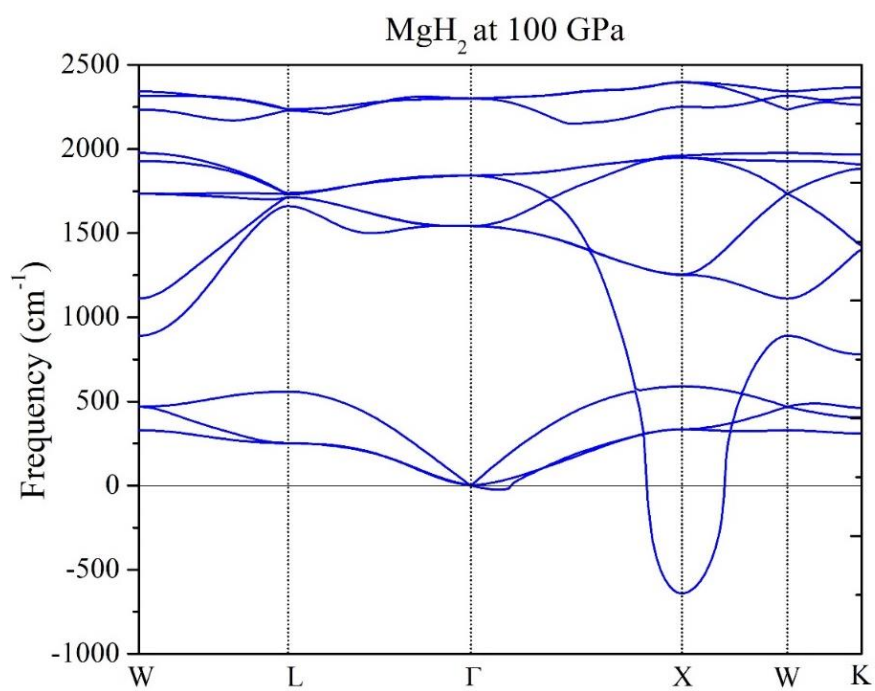
Figure 17 Phonon dispersion of MgH_2 at 100 GPa
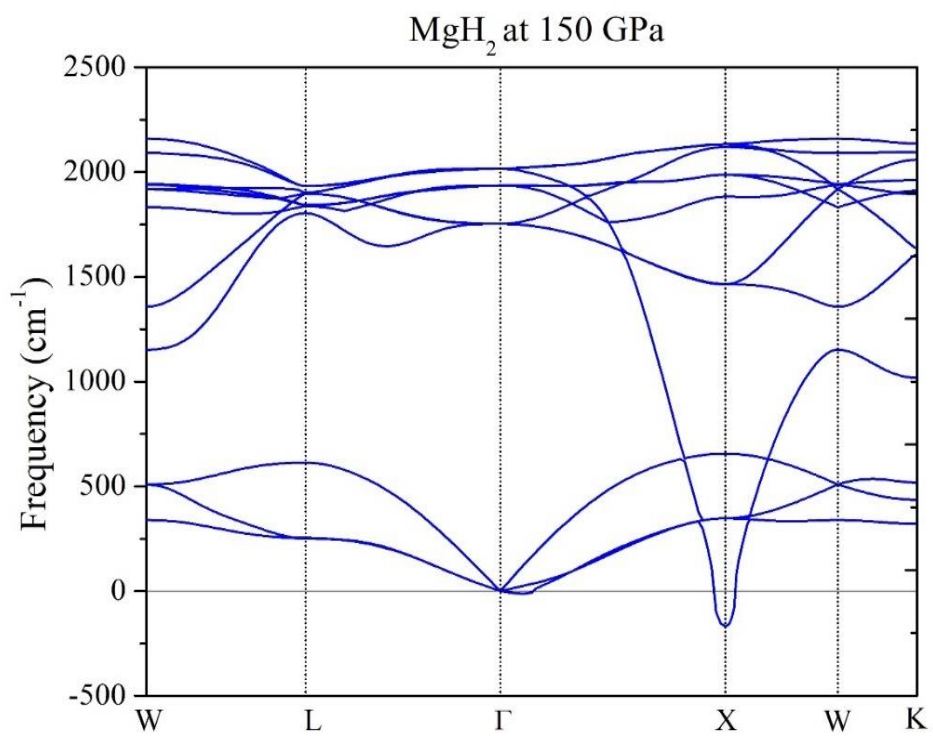
MgH$_2$ at 150 GPa

Figure 18 Phonon dispersion of MgH$_2$ at 150 GPa
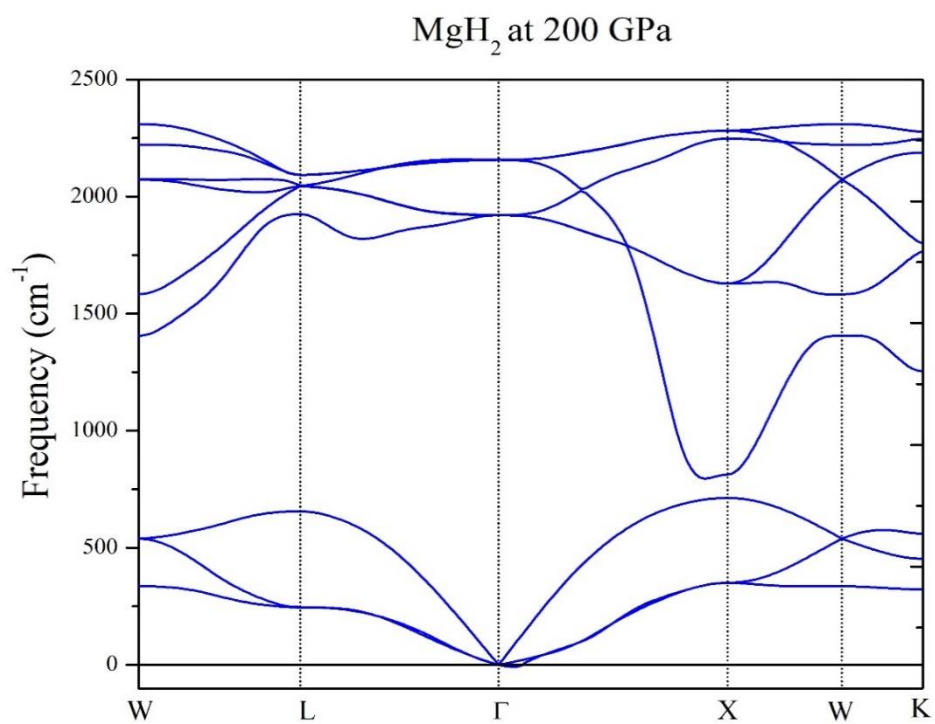
MgH$_2$ at 200 GPa

Figure 19 Phonon dispersion of MgH$_2$ at 200 GPa

The results of the calculations occur the same way at other pressures. Figure 17, 18 and 19 show the MgH_2 phonon frequency at 100, 150, and 200 GPa. The results indicate that a part of the phonon frequency is negative, implying that the phonon dispersion is unstable. We tried raising the k point resolution to 24 x 24 x 24, but the phonon result remained negative. However, the test results of the MgD_2 structure at 100, 150, and 200 GPa cannot give the results of the calculations by using the same variables. Therefore, we focus on the next structures which are MgH_3 and MgD_3.
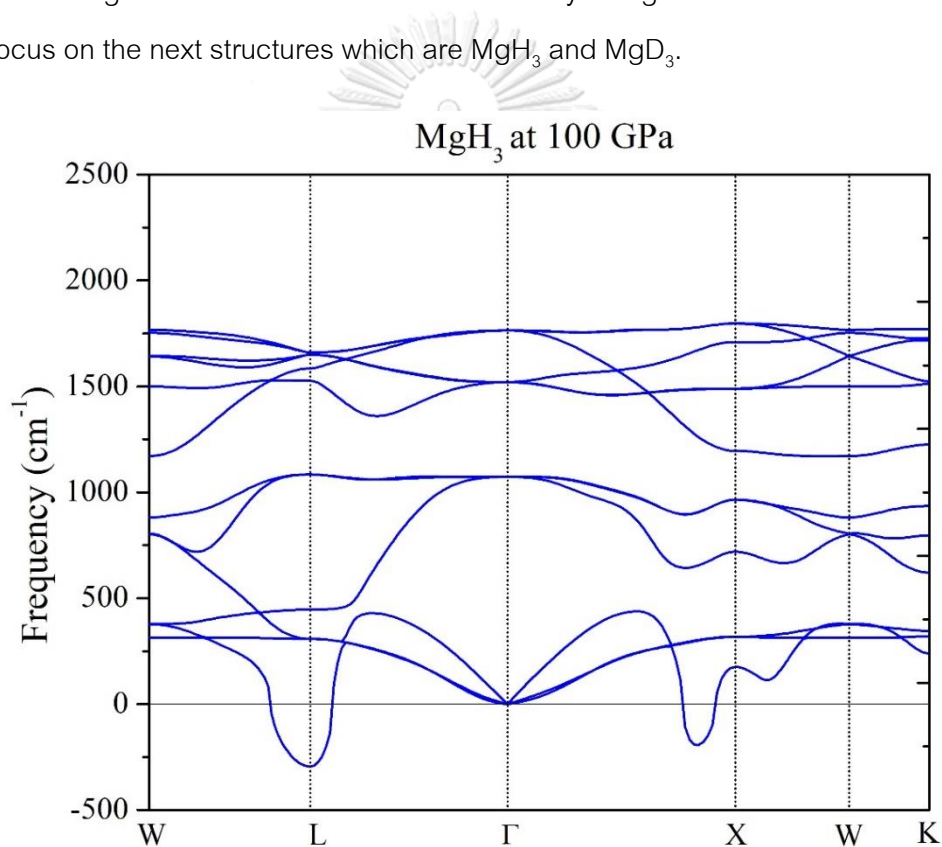
Figure 20 Phonon dispersion of MgH_3 at 100 GPa

From the phonon calculation in figure 20, the results of Phonon dispersion of MgH_3 at 100 GPa show that the frequency of phonon in Fm-3m structure of MgH_3 at 100 GPa has negative value. Therefore, the stability of MgH_3 structure under this pressure is unstable. At 150 GPa and above, MgH_3 becomes more energetically favorable than MgH_2.The phonon dispersion of MgH_3 structure at 150 and 200 GPa are showed in figure 21 and

22 and we discovered that the phonon frequency of MgH_3 increases as pressure increases. The increased pressure on the structures increases the frequencies of all modes, but the magnitude of the increase varies. The high frequency modes show a significant shift in frequency with pressure, whereas the acoustic modes are almost unchanged. This means that pressure has no influence on the effective force constants for the low frequency modes, or even slightly decreases them.
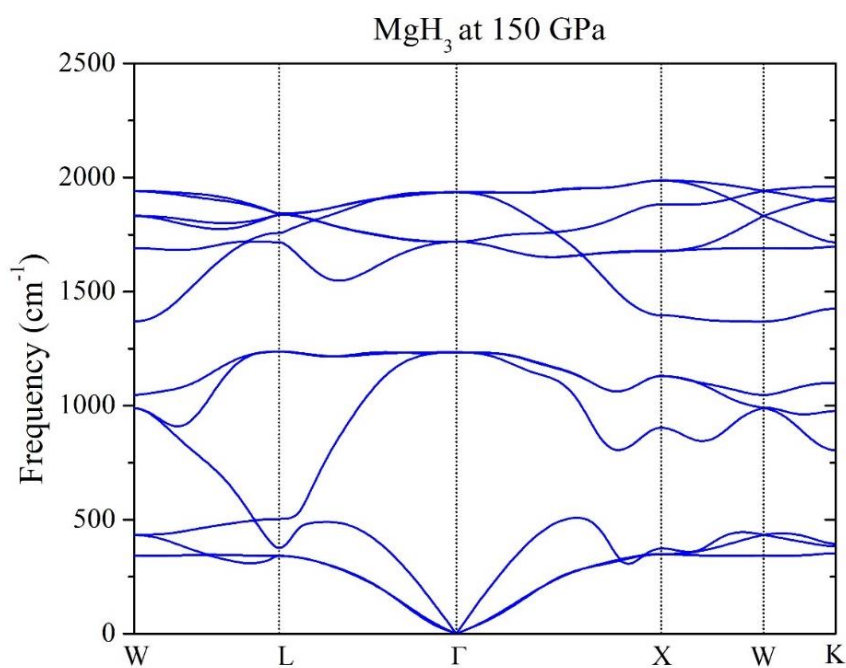
Figure 21 Phonon dispersion of MgH_3 at 150 GPa
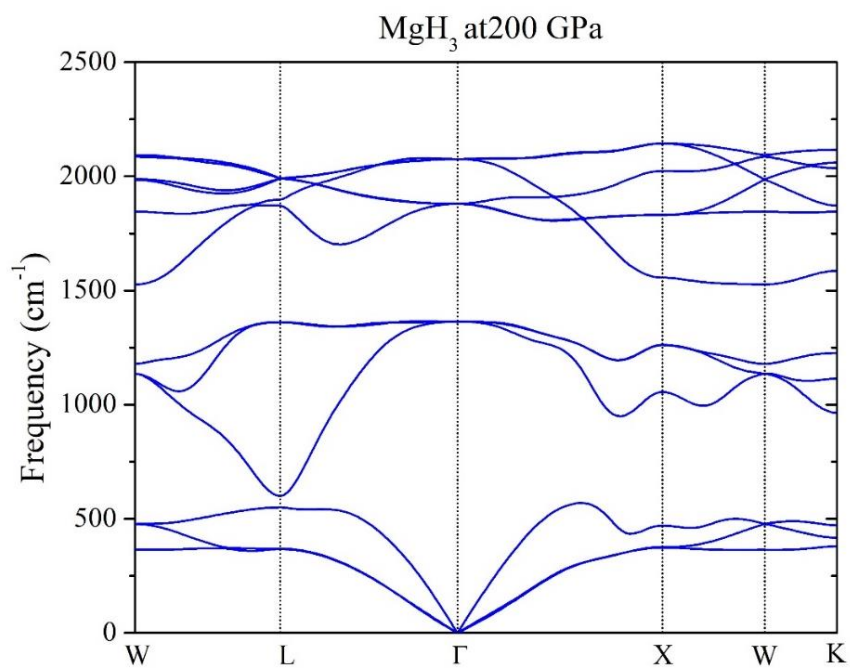
MgH$_3$ at 200 GPa

Figure 22 Phonon dispersion of MgH$_3$ at 200 GPa
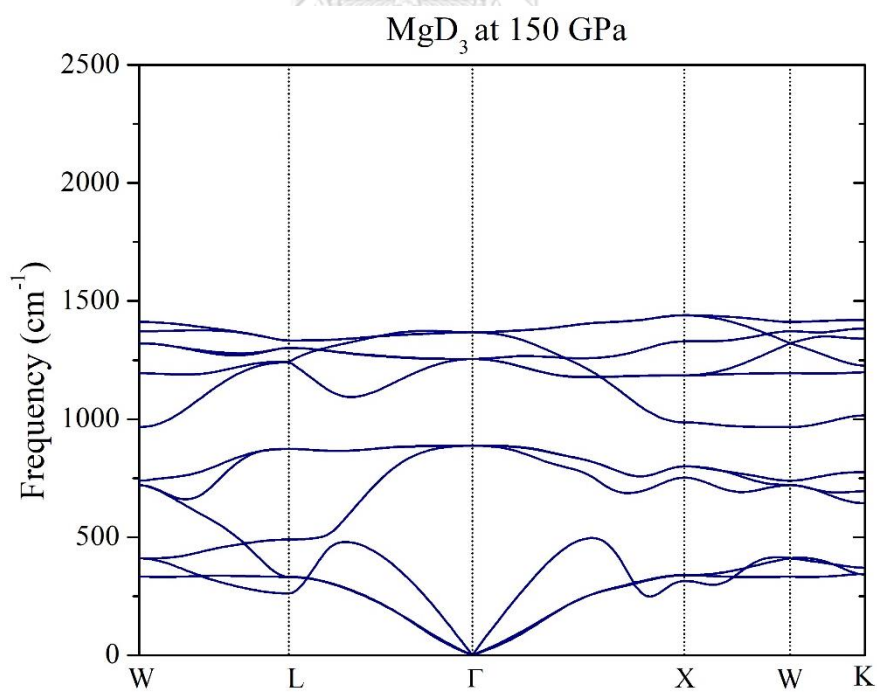
MgD$_3$ at 150 GPa

Figure 23 Phonon dispersion of MgD$_3$ at 150 GPa
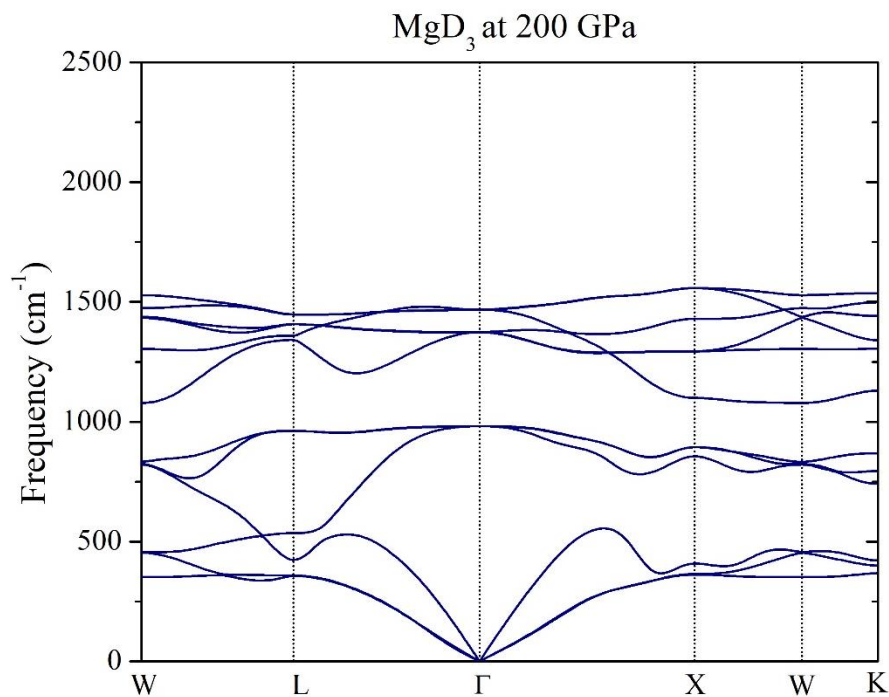
Figure 24 Phonon dispersion of MgD$_3$ at 200 GPa

In figure 23 and 24 the results of the calculations occur the same way at MgD$_3$ structure, the phonon dispersion results show that all the frequency of phonon in Fm-3m structure of MgD$_3$ at 150 and 200 GPa have positive value and when pressure is increased, the phonon frequency also increases, like in MgH$_3$, although the optical mode of MgD$_3$ is lower than the optical mode of MgH$_3$. As a result, the MgD$_3$ structure is assumed to be stable over this operating pressure.
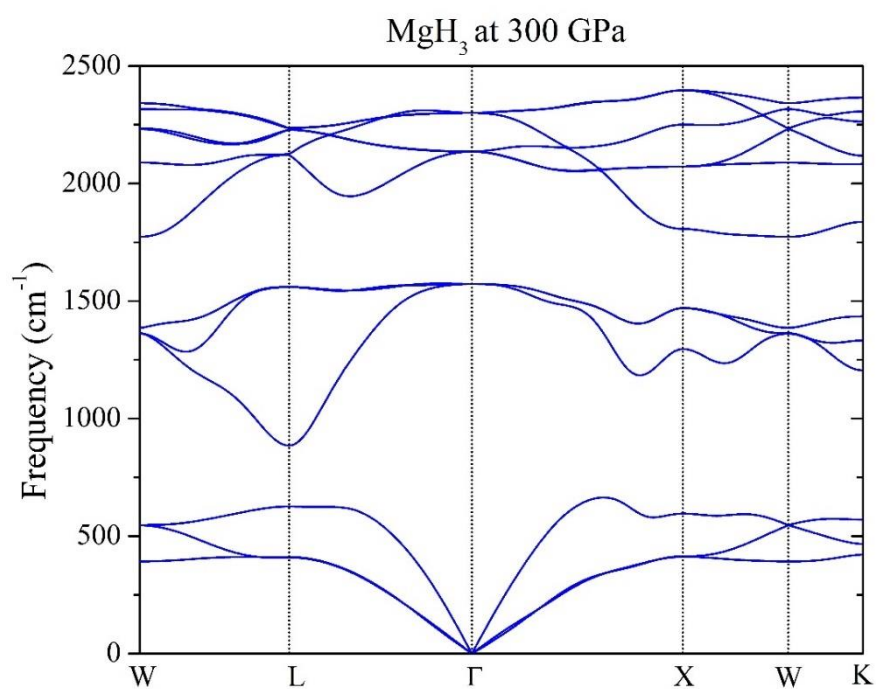
Figure 25 Phonon dispersion of MgH$_3$ at 300 GPa
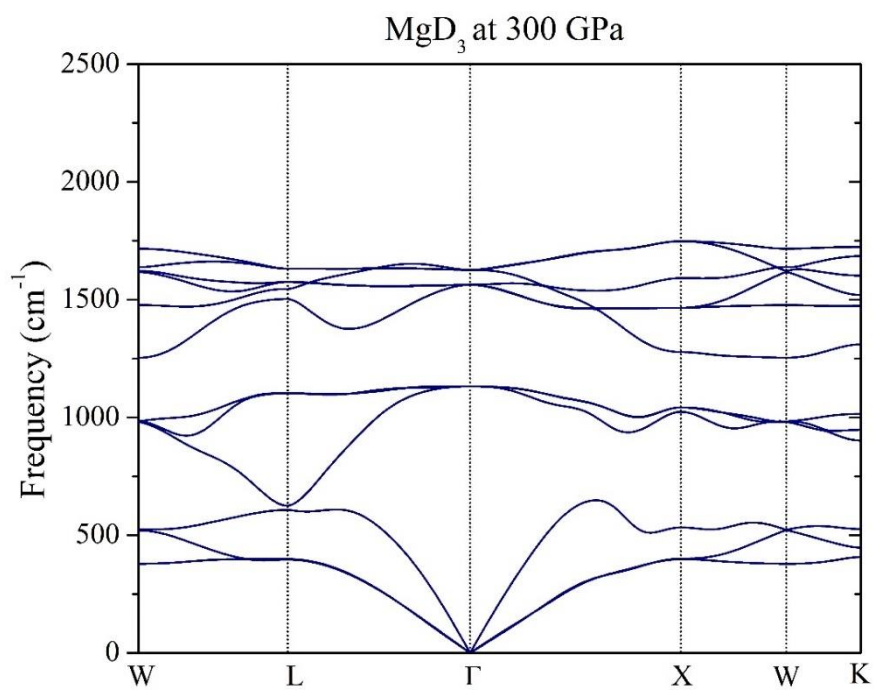
Figure 26 Phonon dispersion of MgD$_3$ at 300 GPa

Figures 25 and 26 illustrate two examples of phonon dispersion at 300 GPa. At the same k point, the phonon frequencies of H of MgH_3 are higher than those of D of MgD_3. This is the so-called isotope effect [25], which may be seen when hydrogen atoms (H) are substituted with deuterium atoms (D). Deuterium is actually twice as heavy as hydrogen in terms of mass. As a result, the phonon frequencies containing hydrogen atom vibrations are $\sqrt{2}$ times greater than those involving deuterium atom vibrations as $\omega \propto \dfrac{1}{\sqrt{m}}$. The phonon frequencies below 750 cm^{-1} in figure 25 belong to the vibrations of the Mg atoms, according to a detailed examination. In Figure 26, these frequencies are mainly preserved. The phonon frequencies in figure 25 above 750 cm^{-1}, on the other hand, correspond to hydrogen atom vibrations. Figure 26's related modes have a frequency that is $\dfrac{1}{\sqrt{2}}$ time of figure 25's. These are caused by the heavier deuterium atoms' vibrations. Future superconducting critical temperature calculations will be based on these phonon dispersion studies.

4.3 The electronic band structures

The band gap in conductors, insulators and semiconductors refers to the energy difference (in electron volts) between the top of the valence band and the bottom of the conduction band in graphs of the electronic band structure of materials. Therefore, the band gap is an important factor in determining a solid's electrical properties. In the first Brillouin zones, the examined band structures for all phases along their high symmetry directions (W-L-G-X-W-K) in the energy range -12 eV to 12 eV and the Fermi energy is set to zero in all of the plots. Figure 27 shows the band structure of MgH_2 at 0 GPa and electronic density of states (DOS) which the character of the bands crosses the Fermi level and the calculation of MgD_2 at 0 GPa show in figure 28 which give the same result as MgH_2. The calculations show that the valence and conduction bands in MgH_2 and MgD_2 structure have an indirect band gap overlap. This indicates that they are metallic. However, this calculation at zero pressure uses the PBE-GGA, which tends to underestimate band gaps [35].
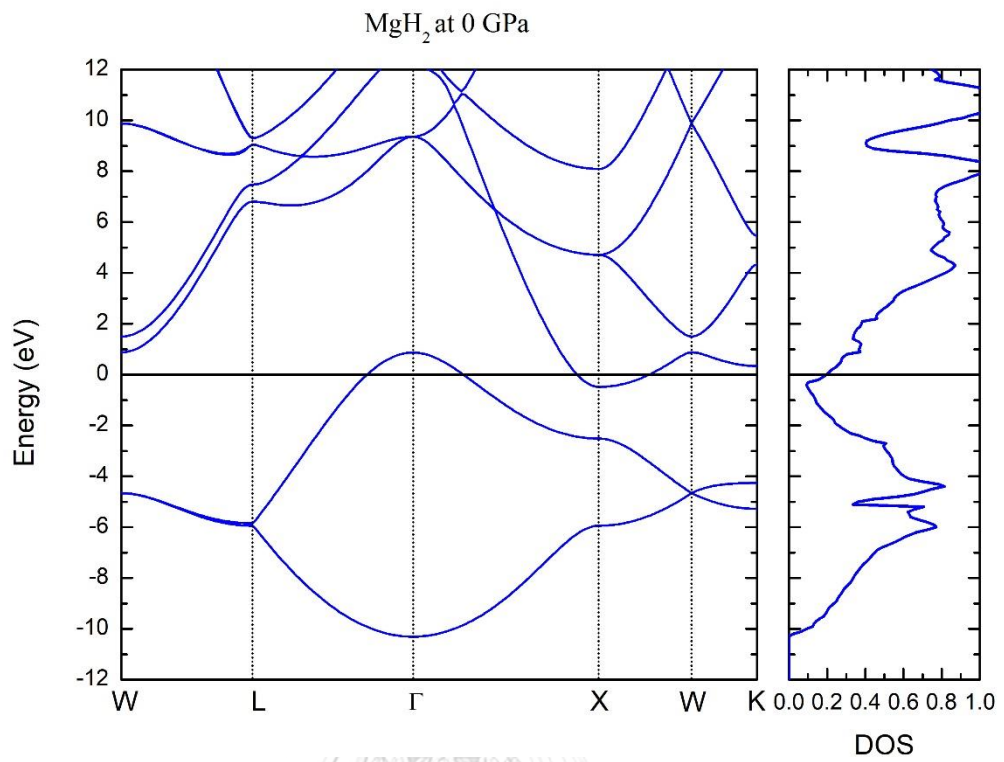
MgH$_2$ at 0 GPa

Figure 27 The electronic band structures of MgH$_2$ at 0 GPa
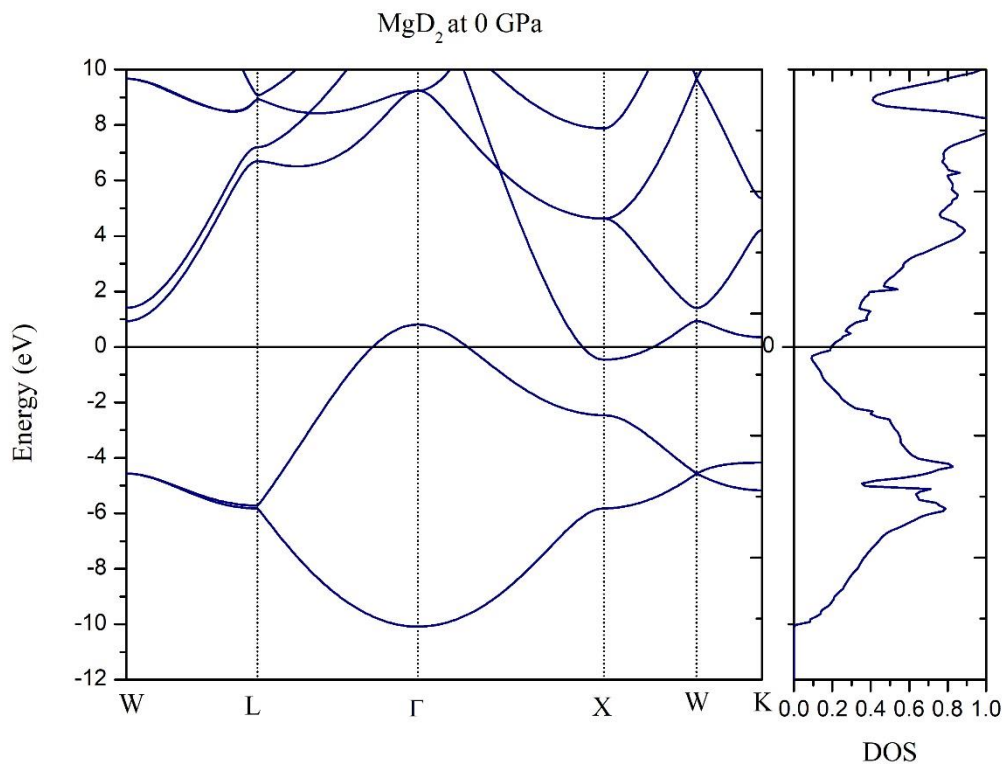
Figure 28 The electronic band structures of MgD$_2$ at 0 GPa

When we calculate the energy band gap at higher pressure as in the example in figure 29, which is the result of MgH$_2$ at 150 GPa and figure 30 which is the result of MgD$_2$ at 150 GPa. They found that the characteristics of the energy band gap were still overlapped and when pressure is increased, the band structure also increases. The band minimum near the Fermi level is at X point with associated with Mg atom and the band maximum is at gamma point associated with H atom. This indicates that MgH$_2$ and MgD$_2$ at 150 GPa behave as metallic in nature, but the calculation is from PBE-GGA, which can underestimate band structure. Unfortunately, these structures turned out to be unstable in the phonon calculation from the results mentioned in phonon dispersion results.
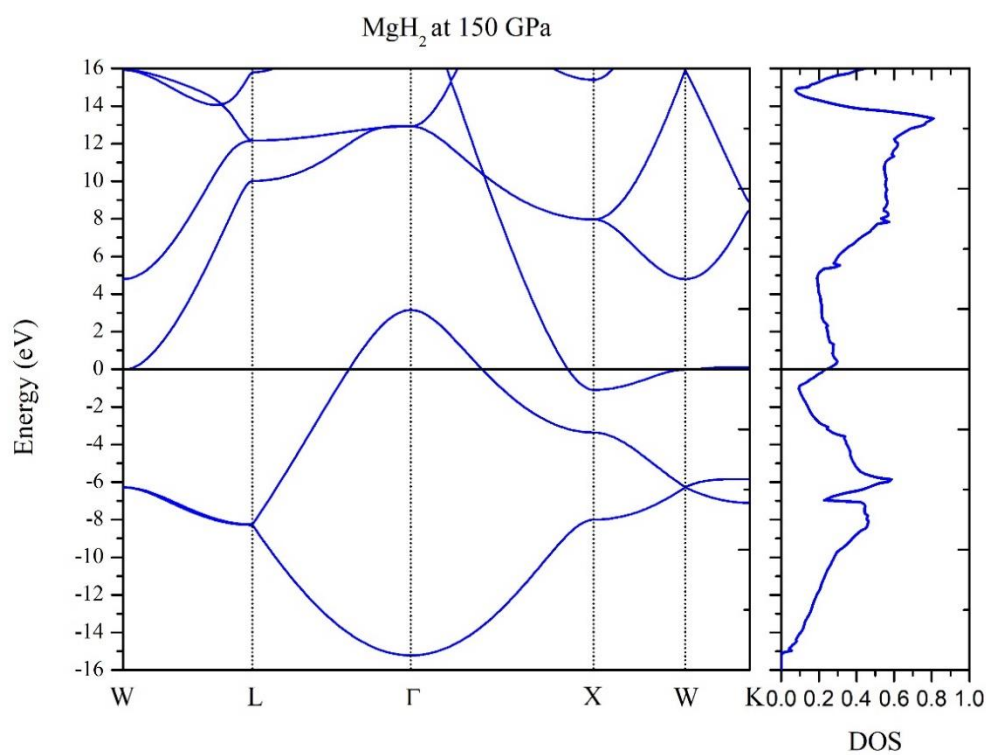
MgH$_2$ at 150 GPa

Figure 29 The electronic band structures of MgH$_2$ at 150 GPa
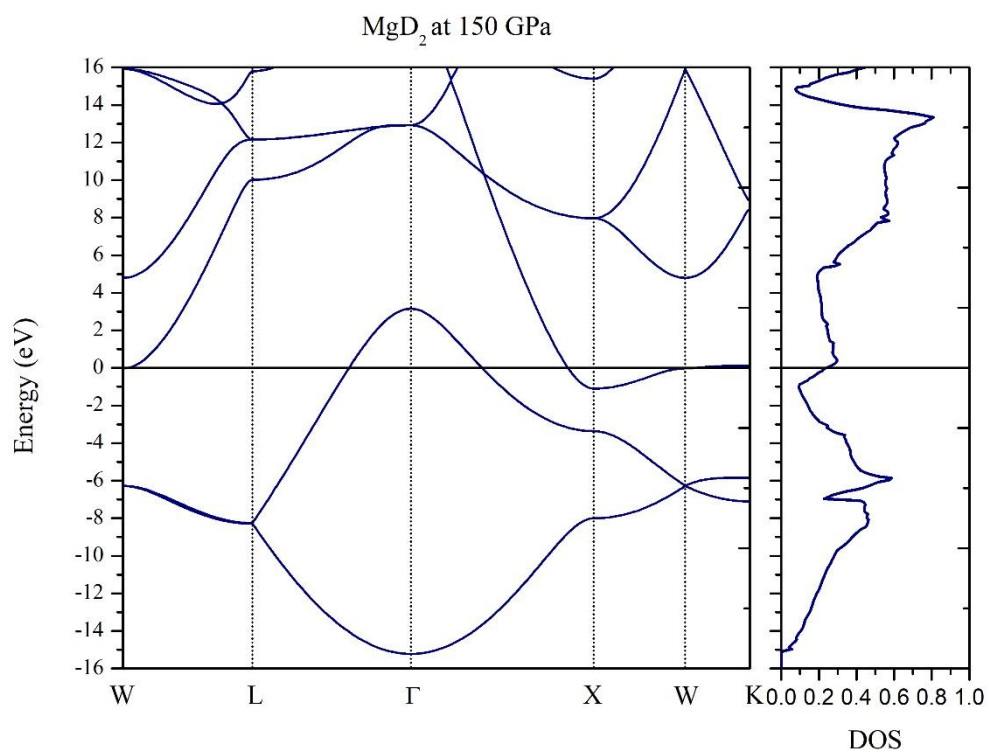
MgD$_2$ at 150 GPa

Figure 30 The electronic band structures of MgD$_2$ at 150 GPa

We also estimated the electronic band structure of MgH_3 and MgD_3 at pressures ranging from 150 to 300 GPa, which are stable due to the convex hull. Figures 31 and 32 show an example of the electronic band structure and electronic density of states (DOS) of MgH_3 and MgD_3 at 150 GPa. The valence bands cross the Fermi level and overlap with the conduction bands, as shown by the electronic structures and their DOS. Near the Fermi level, the band minimum is at the W point associated with the Mg atom, while the band maximum is at the gamma point associated with the H atom. As a result, under pressure, MgH_3 and MgD_3 are metallic. However, there is no difference between the electronic structures of MgH_3 and MgD_3 at this level of DFT computations. The results of MgH_3 and MgD_3 are still metallic under pressure at 300 GPa and also give the exact same value of energy band structure and density of state as shown in figure 33 and figure 34.
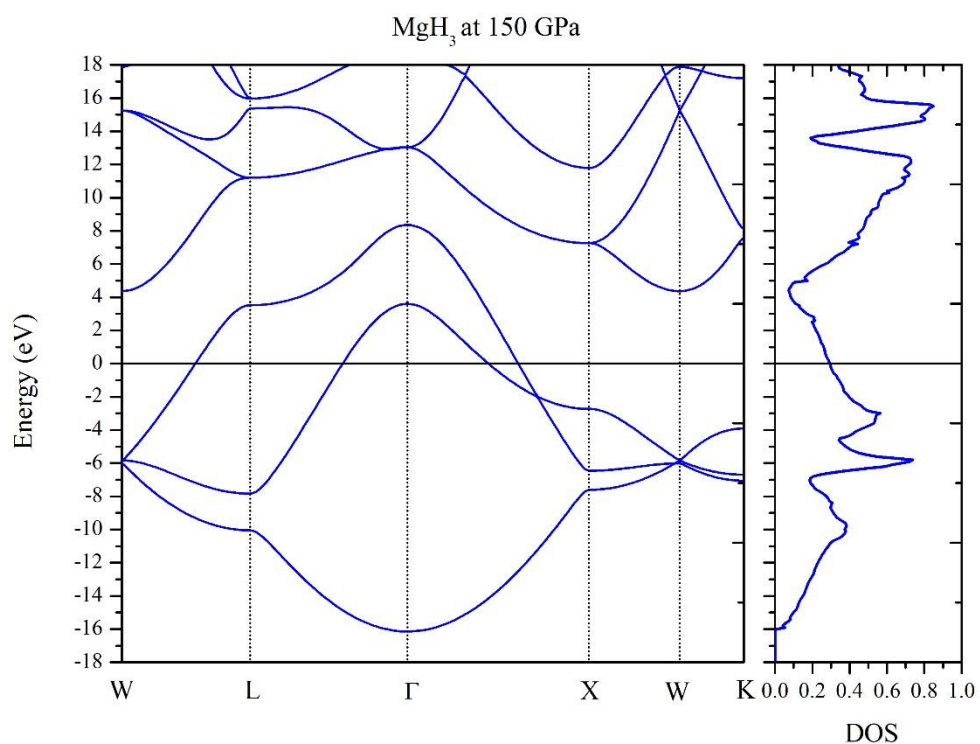
Figure 31 The electronic band structures of MgH_3 at 150 GPa
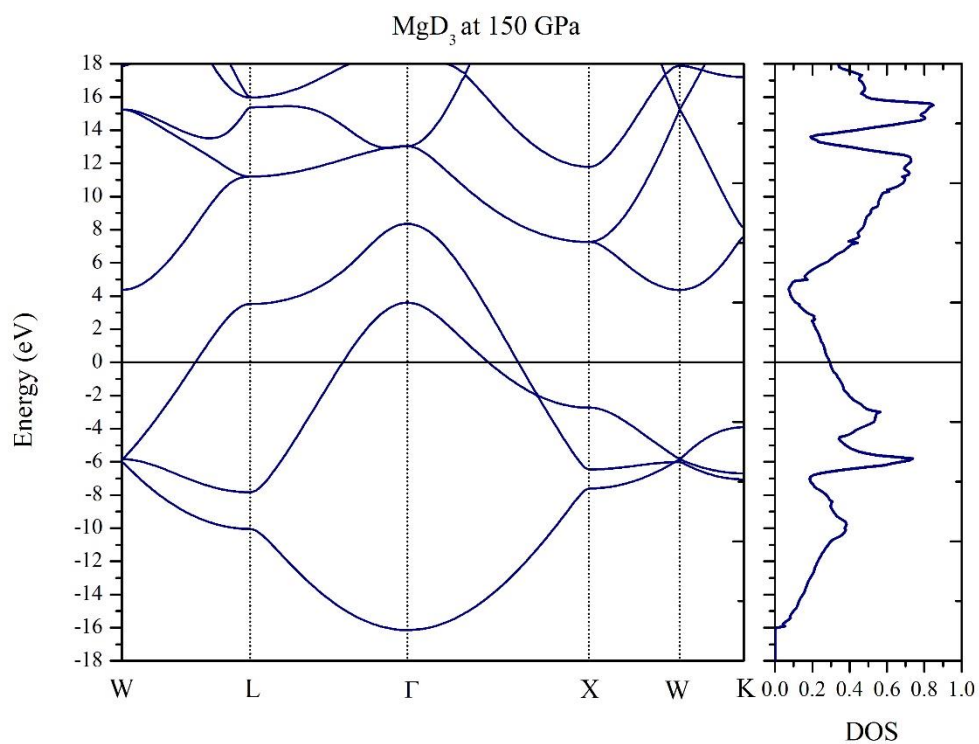
MgD$_3$ at 150 GPa

Figure 32 The electronic band structures of MgD$_3$ at 150 GPa
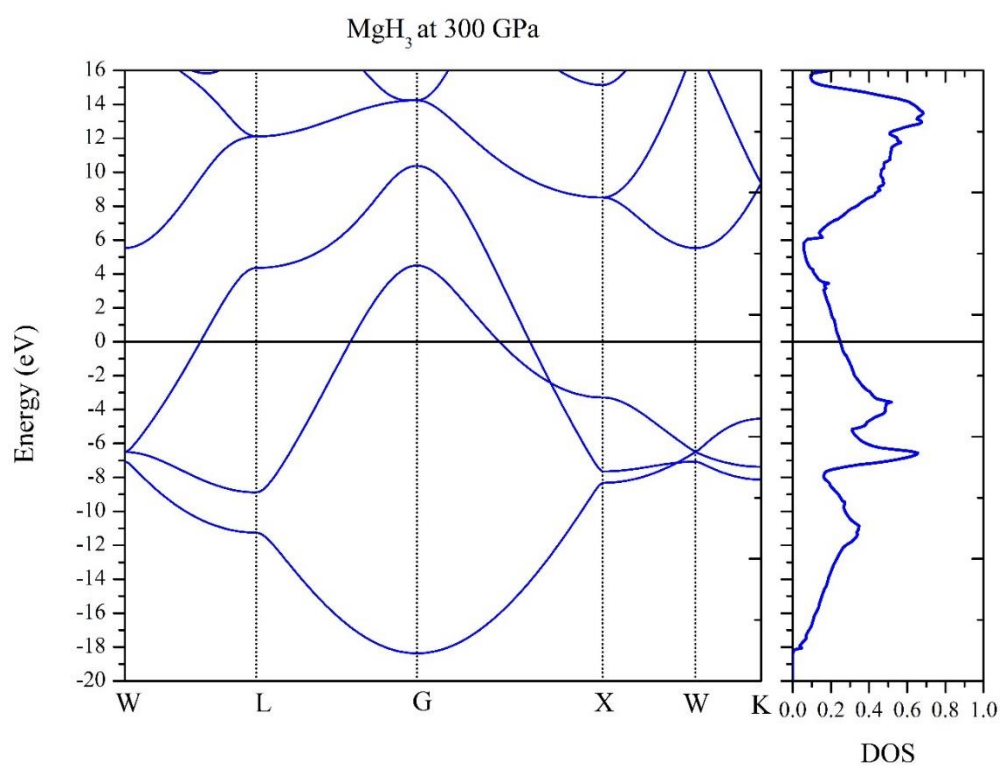
MgH$_3$ at 300 GPa

Figure 33 The electronic band structures of MgH$_3$ at 300 GPa
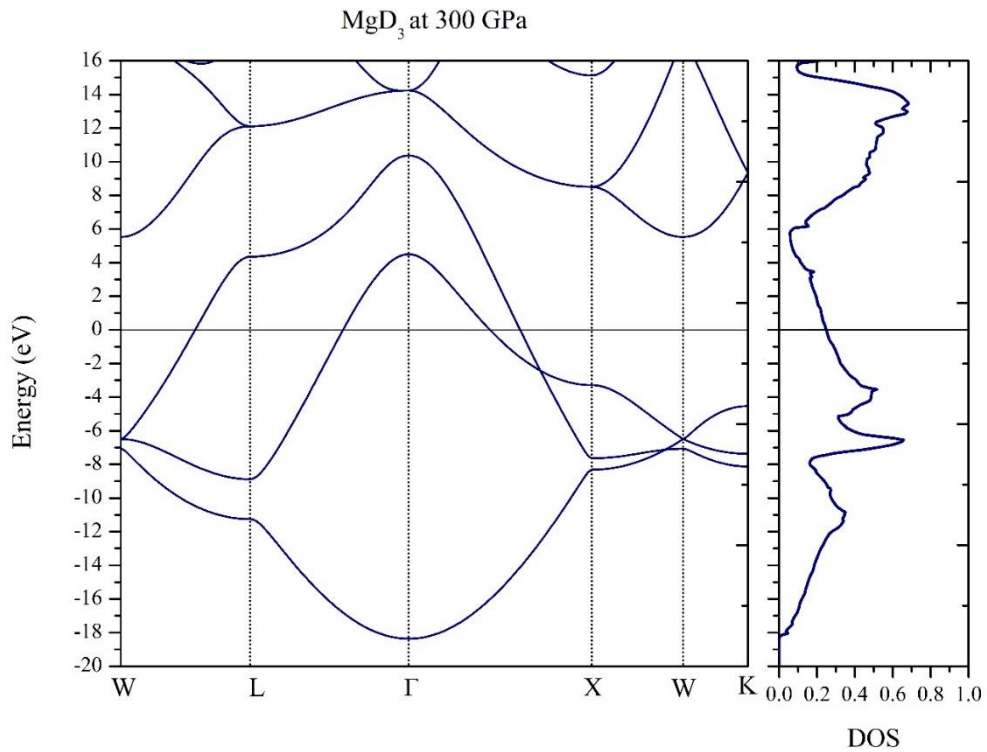
Figure 34 The electronic band structures of MgD$_3$ at 300 GPa

In the future, the work that can be extended in this work is to determine the critical temperature. The critical temperature is related $T_c \propto \omega_D e^{-\frac{1}{N_F V}}$. ω_D is the Debye frequency which relate to the phonon dispersion. N_F is the density of electron at the Fermi level which relate to the electronic structure of this work. V is the electron-phonon interaction. However, V is computationally costly and will be investigated further in the future.

5. CONCLUSIONS AND SUGGESTIONS

In this research, we have calculated the convex hull of MgH_2(FCC), MgH_2(HCP) and MgH_3 under pressure from 0–300 GPa by using DFT. We observed that MgH_2(HCP) is unstable at all pressures, while MgH_3 is stable between 100 - 300 GPa and becomes more energetically favorable than MgH_2(FCC) from 150 GPa. Between 0 - 200 GPa, MgH_2(FCC) is thermodynamically stable so we removed MgH_2(HCP) from the remaining of the calculation. The phonon calculations confirmed that MgH_3 is dynamically stable at high pressure, and due to the isotope effect, the phonon frequencies of MgD_3 are $\frac{1}{\sqrt{2}}$ times lower than those of MgH_3. However, even after increasing the computational resolution, the MgH_2 and MgD_2 results are unstable under pressures ranging from 0 to 200 GPa. The electrical band structures of MgH_3 and MgD_3 and electronic density of states (DOS) were also described, which appear to be identical including MgH_2 and MgD_2 as well. As a result of having the same potential but the weight of deuterium has no effect on the electrical band structures and electronic density of states. For suggestion, at zero pressure, PBE-GGA can underestimate band structure so we may use the new functional in band structure calculation which are significantly more accurate with experiment such as the GGA suggested by Engle and Vosko and the modified Becke-Johnson exchange correlation potential by Trans and Blaha [36]. And we suggest that partial density of states (PDOS) can use to describe the contribution at Fermi level better than the density of state for the future work.

REFERENCES

1.	Onnes, H.K. *The resistance of pure mercury at helium temperatures. Further experiments with liquid helium. IV*. in *Proceedings Koninklijke Akademie van Wetenschappen te Amsterdam*. 1911.

2.	Schilling, A., et al., *Superconductivity above 130 k in the hg–ba–ca–cu–o system*. Nature, 1993. **363**(6424): p. 56-58.

3.	Wu, G., et al., *Superconductivity at 56 K in samarium-doped SrFeAsF*. Journal of Physics: Condensed Matter, 2009. **21**(14): p. 142203.

4.	Nagamatsu, J., et al., *Superconductivity at 39 K in magnesium diboride*. nature, 2001. **410**(6824): p. 63-64.

5.	Reichlin, R., et al., *Evidence for the insulator-metal transition in xenon from optical, x-ray, and band-structure studies to 170 GPa*. Physical review letters, 1989. **62**(6): p. 669.

6.	Gao, L., et al., *Superconductivity up to 164 K in HgBa 2 Ca m⚊ 1 Cu m O 2 m+ 2+ δ (m= 1, 2, and 3) under quasihydrostatic pressures*. Physical Review B, 1994. **50**(6): p. 4260.

7.	Wigner, E. and H.á. Huntington, *On the possibility of a metallic modification of hydrogen*. The Journal of Chemical Physics, 1935. **3**(12): p. 764-770.

8.	Ashcroft, N., *Hydrogen dominant metallic alloys: high temperature superconductors?* Physical Review Letters, 2004. **92**(18): p. 187002.

9.	Pinsook, U., *In search for near-room-temperature superconducting critical temperature of metal superhydrides under high pressure: A review*. Journal of Metals, Materials and Minerals, 2020. **30**(2).

10.	Sukmas, W., et al., *Near-room-temperature superconductivity of Mg/Ca substituted metal hexahydride under pressure*. Journal of Alloys and Compounds, 2020. **849**: p. 156434.

11.	Galey, B., et al., *Improved hydrogen storage properties of Mg/MgH2 thanks to the addition of nickel hydride complex precursors*. International Journal of Hydrogen

Energy, 2019. **44**(54): p. 28848-28862.

12. Yodpradit, K., *Advanced Hydrogen Storage*, in *Medium*. 2020.

13. Hohenberg, P. and W. Kohn, *Inhomogeneous electron gas.* Physical review, 1964. **136**(3B): p. B864.

14. Kohn, W. and L.J. Sham, *Self-consistent equations including exchange and correlation effects.* Physical review, 1965. **140**(4A): p. A1133.

15. Giannozzi, P., et al., *QUANTUM ESPRESSO: a modular and open-source software project for quantum simulations of materials.* Journal of physics: Condensed matter, 2009. **21**(39): p. 395502.

16. Blöchl, P.E., O. Jepsen, and O.K. Andersen, *Improved tetrahedron method for Brillouin-zone integrations.* Physical Review B, 1994. **49**(23): p. 16223.

17. Born, M. and R. Oppenheimer, *Zur quantentheorie der molekeln.* Annalen der physik, 1927. **389**(20): p. 457-484.

18. Bassani, F., *Encyclopedia of condensed matter physics*. 2005: Elsevier acad. press.

19. Perdew, J.P. and Y. Wang, *Accurate and simple analytic representation of the electron-gas correlation energy.* Physical review B, 1992. **45**(23): p. 13244.

20. Bloch, F., *Über die quantenmechanik der elektronen in kristallgittern.* Zeitschrift für physik, 1929. **52**(7): p. 555-600.

21. Blöchl, P.E., *Projector augmented-wave method.* Physical review B, 1994. **50**(24): p. 17953.

22. Li, J. and I. Yip, *Handbook of materials modeling.* Yip. Chapter 2.8 Basic Molecular Dynamics, 2005: p. 565-588.

23. Monkhorst, H.J. and J.D. Pack, *Special points for Brillouin-zone integrations.* Physical review B, 1976. **13**(12): p. 5188.

24. Sherrill, C.D., *An introduction to Hartree-Fock molecular orbital theory.* School of Chemistry and Biochemistry Georgia Institute of Technology, 2000.

25. Pfrommer, B.G., et al., *Relaxation of crystals with the quasi-Newton method.* Journal of Computational Physics, 1997. **131**(1): p. 233-240.

26. Jiles, D., *Introduction to the electronic properties of materials*. 2017: CRC Press.

27. Togo, A. and I. Tanaka, *First principles phonon calculations in materials science.* Scripta Materialia, 2015. **108**: p. 1-5.

28. Bardeen, J., L.N. Cooper, and J.R. Schrieffer, *Theory of superconductivity.* Physical review, 1957. **108**(5): p. 1175.

29. Szczęśniak, R. and A. Durajski, *The isotope effect in H3S superconductor*. Solid State Communications, 2017. **249**: p. 30-33.

30. Marsiglio, F., *Eliashberg theory: A short review.* Annals of Physics, 2020. **417**: p. 168102.

31. Morel, P. and P. Anderson, *Calculation of the superconducting state parameters with retarded electron-phonon interaction*. Physical Review, 1962. **125**(4): p. 1263.

32. Hobbs, D., G. Kresse, and J. Hafner, *Fully unconstrained noncollinear magnetism within the projector augmented-wave method.* Physical Review B, 2000. **62**(17): p. 11556.

33. Shao, Z., et al., *Ternary superconducting cophosphorus hydrides stabilized via lithium.* npj Computational Materials, 2019. **5**(1): p. 1-8.

34. Wang, Z. and X. Ruan, *Phonon spectral energy density analysis of solids: The k point reduction in the first Brillouin zone of FCC crystals and a case study on solid argon.* Computational Materials Science, 2016. **121**: p. 97-105.

35. Pickard, C.J. and R. Needs, *Metallization of aluminum hydride at high pressures: A first-principles study.* Physical Review B, 2007. **76**(14): p. 144114.

36. Zarshenas, M., et al., *First principle investigations of the physical properties of hydrogen-rich MgH2.* Physica Scripta, 2013. **88**(6): p. 065704.

VITA

NAME	นาย ชยพล บุญโชติ
DATE OF BIRTH	14 กันยายน 2539
PLACE OF BIRTH	ตรัง
INSTITUTIONS ATTENDED	ปริญญาตรี
HOME ADDRESS	130/9 ถ.วิเศษกุล ต.ทับเที่ยง อ. เมือง จ.ตรัง